

Cosmic Voids and Biased Galaxy Formation

Blane Little¹ and David H. Weinberg²

¹ *Astronomy Unit, School of Mathematical Sciences, Queen Mary and Westfield College,
Mile End Road, London E1 4NS*

² *Institute for Advanced Study, Olden Lane, Princeton, New Jersey, 08540 U.S.A.*

e-mail: bl@starlink.qmw.ac.uk, dhw@guinness.ias.edu

Abstract

Using cosmological N -body simulations and the void probability function (VPF), we investigate the statistical properties of voids within a wide range of initially Gaussian models for the origin of large-scale structure. We study the dependence of the VPF on cosmological parameters, on the power spectrum of primordial fluctuations, and on assumptions about galaxy formation. We pay particular attention to the ability of the VPF to diagnose ‘biased galaxy formation’: the preferential formation of galaxies in regions of high background density and corresponding suppression of galaxy formation in regions of low background density. We find that the VPF is insensitive to the cosmic density parameter Ω_0 and the cosmological constant λ_0 , provided that fluctuations are normalized to a fixed rms amplitude on scales $\sim 8 h^{-1}$ Mpc. In the absence of biasing, the VPF is also insensitive to the shape of the initial power spectrum. The VPF does depend on the prescription adopted for biased galaxy formation, in the obvious sense that a scheme that more efficiently suppresses galaxy formation in low density regions leads to larger voids. Biased models have systematically higher VPFs than unbiased models, but for a given biasing scheme the VPF is relatively insensitive to the value of the bias factor b , the ratio of rms galaxy fluctuations to rms mass fluctuations. Thus, while the VPF can distinguish unbiased models from some biased models, it is probably not a useful way to constrain the bias factor; uncertainties in the appropriate choice of biasing prescription overwhelm the mild dependence on b .

We compare the predictions of our models to the most extensive VPF observations published to date. These data do *not* require strong biasing; Gaussian models in which galaxies trace mass can reproduce the VPF data to within the errors expected from the current finite volume fluctuations. Models with the moderate biasing predicted by cosmological simulations that incorporate gas dynamics yield a slightly better match to the data. Models in which galaxy formation is strongly suppressed in low density regions produce an excess of large, empty voids.

arXiv:astro-ph/9306006v1 11 Jun 1993

1. Introduction

Giant voids are among the most striking features of the observed distribution of galaxies (*e.g.* Gregory & Thompson 1978; Kirshner *et al.* 1981, 1987; Davis *et al.* 1982; de Lapparent, Geller & Huchra 1986; see review by Rood 1988 and references therein). The remarkable interlocking pattern of superclusters and voids revealed by galaxy redshift surveys has prompted various authors to describe the observed galaxy distribution as a “cell structure” (Joeveer & Einasto 1978), a foam of “bubbles” (de Lapparent, Geller & Huchra 1986), or a “sponge-like” network of interlocking filaments and tunnels (Gott, Melott & Dickinson 1986). The most widely explored models for the origin of large-scale structure propose that the clusters, superclusters, and voids that we observe today developed by gravitational instability from small-amplitude, Gaussian fluctuations, generated by physical processes in the very early universe. Can the gravitational growth of Gaussian primordial fluctuations account for the observed voids, or do these models require that galaxy formation be suppressed in low density regions in order to produce voids as large and empty as observed? Do voids represent regions where there is no mass, or merely regions where there are no (bright) galaxies? In this paper we address these questions using cosmological N -body simulations and the void probability function (VPF), a simple statistical measure of the sizes of voids. The VPF of a galaxy sample is the probability $P_0(R)$ that a randomly placed sphere of radius R contains no galaxies. We study the dependence of the VPF on cosmological parameters, on the power spectrum of the primordial fluctuations, and – above all – on assumptions about galaxy formation. We also compare our results to the most extensive VPF observations published to date (Vogeley, Geller & Huchra 1991).

The nature of voids is intimately connected to the issue of ‘biased galaxy formation,’ an idea that first gained popularity in the context of the cold dark matter (CDM) model of structure formation. The most theoretically attractive version of CDM assumes a critical density ($\Omega = 1$) universe. Observations of cluster mass-to-light ratios, cluster velocity dispersions, and the galaxy pairwise velocity dispersion clearly contradict this assumption *if* galaxies are clustered in the same way as mass (*e.g.*, Davis *et al.* 1985, hereafter DEFW). However, if galaxy formation is more efficient (per unit mass) in regions of high background density, then galaxies will cluster more strongly than the underlying mass distribution, and an $\Omega = 1$ model can, perhaps, be reconciled with the observations (DEFW; Bardeen *et al.* 1986, hereafter BBKS). While the term ‘biasing’ might be used to describe any difference between the large-scale galaxy and mass distributions, we will use it in the specific sense mentioned above: preferential formation of galaxies in regions of high background density. If galaxies form more efficiently than average in high density regions, then they must form less efficiently than average in low density regions, so biasing naturally produces voids that are empty of galaxies but not completely empty of mass.

There are observational and theoretical reasons for thinking that biasing might be an important phenomenon, independent of the $\Omega = 1$ assumption. On the observational side, the well known morphology-density relation implies that elliptical and spiral galaxies have different clustering properties (Dressler 1980; Postman & Geller 1984). At least one of these classes of galaxies must cluster differently than the mass, and there is no particular reason to think that either class individually or the union of the two traces the large-scale mass distribution. On the theoretical side, galaxy-scale perturbations collapse earlier in regions of high background density, so they tend to reach higher internal densities and cool more efficiently than equivalent perturbations in low density regions. Indeed, numerical simulations that include gas dynamics indicate that galaxy formation is at least somewhat biased towards regions of high background density (Cen & Ostriker 1992; Katz, Hernquist & Weinberg 1992; see also White *et al.* 1987; Kaiser 1988; Gelb 1992).

It has also been argued that gravity alone cannot create voids as large and empty as those observed, and that the existence of these voids is itself evidence for biased galaxy formation (*e.g.* Dekel & Rees 1987; Betancort-Rijo 1990; Einasto *et al.* 1991, hereafter EEGS). This line of reasoning, if correct, enhances the plausibility of $\Omega = 1$ models by providing independent evidence for biasing, and it suggests that a measure of void sizes like the VPF might offer a sensitive statistical diagnostic of biasing. We will assess the strength of the VPF as a biasing diagnostic, and we will examine the ability of current theoretical models to explain the observed spectrum of void sizes.

There have been several recent N -body studies of the gravitational growth and interactions of voids, in idealized configurations (Dubinski *et al.* 1993; see also West, Weinberg & Dekel 1990), in void-dominated structure models (Regös & Geller 1991), and in models with Gaussian initial conditions (van de Weygaert & van Kampen 1993). These papers did not examine the void probability function or the effects of biased galaxy formation, which will be the central concerns of our investigation. The two most direct predecessors of the present study are the above cited work by EEGS and the paper by Weinberg & Cole (1992; hereafter WC). The latter applied the VPF (and other clustering statistics) to N -body models with Gaussian and non-Gaussian initial conditions. WC found the VPF to be a sensitive discriminant between Gaussian and non-Gaussian models in the absence of biasing, but they found, unsurprisingly, that biasing could create large voids in all models. Gaussian models proved more successful than any of WC’s non-Gaussian models in explaining the full range of galaxy clustering data, and the Gaussian hypothesis has received further observational support from recent analyses of large-scale galaxy counts (Bouchet *et al.* 1993 and references therein). Since Gaussian fluctuations have both theoretical simplicity and a degree of empirical success on their side, we will restrict our attention to Gaussian models in this paper.

Because of our relatively narrow focus, we have been able to improve upon the studies of EEGS and/or WC in a number of ways:

- (1) EEGS’s models were normalized by arranging for them to have the same final rms mass fluctuation on a particular scale. However, the distribution of total (luminous + dark) mass in the real universe is not well-determined. A more meaningful comparison between theory and observation can therefore be obtained if one’s theoretical models are adjusted to share an *observable* property, such as the rms fluctuation in galaxy counts on a particular scale. This is what we do, and it constitutes the most important difference of principle between our study and that of EEGS.
- (2) The initial conditions of N -body simulations cannot include contributions from Fourier density waves that are bigger than the simulation cube, and the enforcement of periodic boundary conditions during N -body evolution prevents such power from developing. A comparable volume of the real universe does not suffer from these restraints. N -body simulations systematically underestimate the frequency of large voids if the simulation volume is not large enough to contain all waves that significantly influence the growth of underdense regions. This limitation may have affected the results of EEGS and WC, whose periodic N -body cubes had sides of 40 and 128 h^{-1} Mpc, respectively ($h \equiv H_0/100$ km s $^{-1}$ Mpc $^{-1}$). By contrast, Kauffmann & Melott (1992) suggest that a CDM simulation would require a ~ 160 h^{-1} Mpc box ‘before one could begin to trust the typical size of voids’. We use simulation cubes that are significantly larger than those of EEGS and WC – either 300 or 192 h^{-1} Mpc on a side. The large simulation volume minimizes the systematic effects of missing large-scale waves, and it reduces the statistical uncertainty in our estimates of the VPF.
- (3) EEGS and WC employ a single biasing prescription, which we shall call ‘density biasing’. Both sets of authors evolve an ensemble of mass points to redshift $z = 0$, smooth the resultant density field, and identify as ‘galaxies’ only those particles above some sharp cutoff in local density. We

also investigate this biasing prescription, but we examine two other biasing schemes as well. One of these is the well-known ‘peaks biasing’ prescription, which identifies galaxies with high peaks of the initial density field (*e.g.*, DEFW; BBKS). For our simulations of the standard CDM model, we also consider the biasing relation derived by Cen & Ostriker (1993) from their hydrodynamic simulations of this scenario. Our three biasing prescriptions differ substantially, and together they span a range of physically relevant possibilities.

- (4) EEGS examined biased versions of only 3 broad types of theoretical models: a distribution of randomly placed galaxies at $z = 0$; a distribution of randomly placed clusters at $z = 0$; and a numerically evolved, spatially flat, Gaussian model with the initial power spectrum of $\Omega_0 = 0.2$ CDM. Only the last of these exhibits the complex clustering characteristic of the observed galaxy distribution. WC evolved 32 theoretical models, but three quarters of them were associated with non-Gaussian initial conditions, and they used only pure power-law initial spectra. We will present some results for power-law spectra, but will concentrate our analysis on initial power spectra with stronger theoretical and empirical motivation. We do not consider non-Gaussian models, but we achieve much better coverage of the most physically promising cosmological models than either WC or EEGS.
- (5) The VPF depends rather sensitively on the number density n of the galaxy sample used to measure it – the sparser the sample, the bigger the voids. While EEGS computed only the VPF, we also compute a related statistic – the underdense probability function (‘UPF’ or P_{80}) – that is independent of n (except for shot noise, which becomes unimportant at large void radii).
- (6) WC examined only two biasing strengths: $b = 1$ (unbiased) and $b = 2$, where b is the ‘bias factor’ defined by the relation $\sigma_{8,\text{galaxies}} = b \sigma_{8,\text{mass}}$. Here σ_8 is the rms fluctuation of the density contrast in randomly placed spheres of radius $8 h^{-1}$ Mpc. While we also explore $b = 1$ and $b = 2$, we investigate two additional biasing strengths of interest ($b = 1.5$ and $b = 3$).
- (7) We improve upon the comparison between theory and observation in three respects:
 - (i) The VPF data are in redshift space, but EEGS and WC compare them with theoretical predictions computed in real space. This can be misleading if the move from real space to redshift space significantly changes the VPF. We compute the VPF both in real space and in redshift space, but – as consistency requires – we compare the VPF data only with redshift-space predictions.
 - (ii) Vogeley, Geller, & Huchra (1991, hereafter VGH) present the most extensive VPF data published to date. Most of these data were unavailable to EEGS, and WC use results from only 2 of VGH’s 12 volume-limited samples. We compare our predictions with all 12 of these samples, some of which extend to $126 h^{-1}$ Mpc. The samples used by WC and EEGS all had limiting depths of $\lesssim 80 h^{-1}$ Mpc.
 - (iii) Unlike both EEGS and WC, we quantify the effects of finite volume errors on current estimates of the VPF.

The next section provides a detailed description of our models, §3 presents our main results, and §4 summarizes our conclusions.

2. The Models

2.1 Initial Conditions

Our basic set of initial conditions consists of an isotropic Gaussian random field (GRF) of density fluctuations, $\delta(\vec{r}) \equiv [\rho(\vec{r}) - \bar{\rho}]/\bar{\rho}$, defined within a triply-periodic simulation cube. Such a field can be expanded in terms of complex Fourier components $\delta_{\vec{k}} = A_{\vec{k}} e^{i\theta_{\vec{k}}}$, and its statistical properties are completely determined by its power spectrum $P(k) \equiv \langle |\delta_{\vec{k}}|^2 \rangle$. For a GRF, the phases $\theta_{\vec{k}}$ are randomly distributed in the interval $[0, 2\pi]$, and the amplitudes $A_{\vec{k}}$ are Rayleigh-distributed with variance $P(k)$. We ensure these conditions by assigning values drawn from a Gaussian distribution with variance $P(k)/2$ separately to the real and imaginary parts of each $\delta_{\vec{k}}$ (cf. BBKS). These Fourier components then allow the computation of a GRF $\delta(\vec{r})$ with a specified power spectrum $P(k)$.

The three cosmological scenarios that we examine in greatest detail have initial power spectra described by equation (7) of Efstathiou, Bond, & White (1992; hereafter EBW), with two different values of their ‘ Γ ’ parameter. With $\Gamma = \Omega_0 h$, this equation provides an accurate fit to the post-recombination, linear power spectrum of adiabatic fluctuations that enter the horizon with scale-invariant amplitudes and grow thereafter in a universe dominated by cold dark matter. Our first model is ‘standard CDM’, with $\Omega = 1$ and $h = 0.5$ (implying $\Gamma = 0.5$). While the standard CDM model has many attractive features, a number of observations suggest that the $\Gamma = 0.5$ spectrum lacks sufficient power on large scales (*e.g.*, Efstathiou *et al.* 1990; Maddox *et al.* 1990; Saunders *et al.* 1991; Moore *et al.* 1992; Vogeley *et al.* 1992; Fisher *et al.* 1993). A better fit to galaxy clustering data is obtained for $\Gamma = 0.25$, and we consider two models with this spectrum. The first is an $\Omega_0 = 0.3$ CDM model, which naturally produces this power spectrum if $h \approx 0.8$. For our standard version of this model we include a cosmological constant, $\lambda_0 \equiv \Lambda/3H_0^2 = 0.7$, so that the spatial curvature vanishes, as predicted by inflationary cosmology (see review by Narlikar & Padmanabhan 1991). We also examine an $\Omega = 1$ model with $\Gamma = 0.25$. There are various physical scenarios that could produce a $\Gamma \approx 0.25$ spectrum in an $\Omega = 1$ universe. They include models in which equalization occurs late because a decaying particle enhances the background neutrino density (*e.g.*, Bond & Efstathiou 1991) or because the Hubble constant is very low. One particularly interesting possibility is a universe dominated by a mixture of hot and cold dark matter – such a model may best explain galaxy clustering and velocity statistics, as well as the microwave background fluctuations recently measured by COBE (*e.g.*, EBW; Davis, Summers & Schlegel 1992; Taylor & Rowan-Robinson 1992; Klypin *et al.* 1993). From a theoretical perspective, all of the proposed models that yield a $\Gamma = 0.25$ spectrum seem somewhat contrived, but one can remain agnostic on the subject of theoretical underpinning and simply view the $\Gamma = 0.25$ spectrum as a reasonably successful empirical fit to observational data.

Figure 1 shows the $\Gamma = 0.5$ and $\Gamma = 0.25$ initial power spectra, extrapolated via linear perturbation theory to $z = 0$ and normalized so that $\sigma_{8,\text{mass}} = 1$, *i.e.*, so that the rms mass fluctuation is unity in randomly placed spheres of radius $8 h^{-1}$ Mpc. The $\Gamma = 0.25$ spectrum has more power on scales larger than this normalization scale. The vertical arrows in this plot indicate the lowest and highest comoving wavenumbers included in our initial conditions: $k/k_f = 1$ (the wavenumber of the fundamental mode of our $300 h^{-1}$ Mpc simulation box) and $k/k_f = 50$ (the Nyquist frequency of the 100^3 grid used to set up our initial conditions). Note that both of the spectra in Figure 1 approach an $n = 1$ power law as $k \rightarrow 0$, in agreement both with inflationary cosmology (see

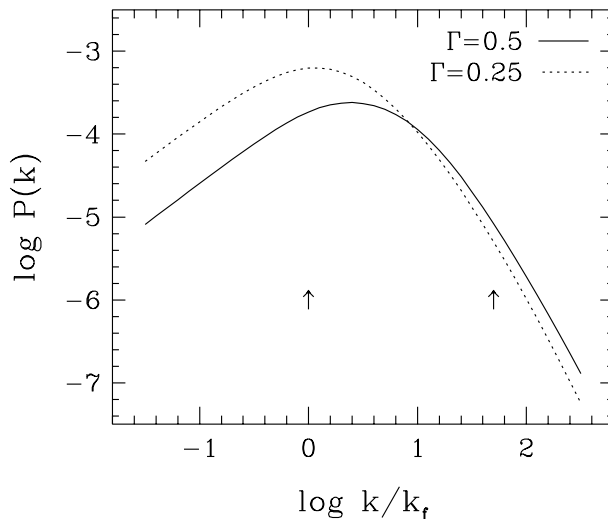


Figure 1 — Initial power spectra for our $\Gamma = 0.5$ and $\Gamma = 0.25$ models. Both spectra have been extrapolated via linear perturbation theory to $z = 0$, and normalized so that the rms mass fluctuation is unity in randomly placed spheres of radius $8 h^{-1}$ Mpc. On scales larger than this, the $\Gamma = 0.25$ spectrum has more power than the $\Gamma = 0.5$ spectrum. Vertical arrows indicate the lowest and highest comoving wavenumbers included in our initial conditions: $k = k_f$ (the wavenumber of the fundamental mode of our $300 h^{-1}$ Mpc simulation box) and $k = 50 k_f$ (the Nyquist frequency of the 100^3 grid used to set up our initial conditions).

Narlikar & Padmanabhan 1991) and with COBE’s recent observations of temperature fluctuations in the cosmic microwave background radiation (Smoot *et al.* 1992).

In order to study the dependence of the VPF on cosmological parameters, we also consider models with the $\Gamma = 0.25$ power spectrum and $(\Omega_0, \lambda_0) = (0.3, 0)$, $(0.1, 0.9)$, and $(0.1, 0)$. We do not change the power spectrum in concert with Ω_0 because we want to separate dependence on cosmological parameters from dependence on the power spectrum. We will show in §3.3 that the VPF is insensitive to Ω_0 and λ_0 if the power spectrum, normalization, and biasing scheme are held fixed. We therefore do not carry out a detailed comparison between these last three models and observational data.

The $\Gamma = 0.25$ and $\Gamma = 0.5$ power spectra are not radically different over the range of scales probed by our simulations. We want to study the dependence of the VPF on the shape of the initial spectrum using a somewhat larger lever arm than these models provide, so we also examine models with pure power-law initial spectra, $P(k) \propto k^n$. A pure power-law spectrum that failed to turn over or cut off would violate observational constraints on either very large or very small scales, but a power law might be a reasonable approximation to the true power spectrum over some finite range. ‘Standard CDM’ predicts a post-recombination power spectrum approximately like $P(k) \propto k^{-1}$ on comoving scales $\sim 3 - 10 h^{-1}$ Mpc, and a variety of observations support this prediction (Gott & Rees 1975; Gott & Turner 1977; Bhavsar, Gott & Aarseth 1981; Gunn 1982; Gott *et al.* 1989, 1992). For our power-law spectra, we therefore consider $n = -1$ and its ‘bracketing values’ of $n = -2$ and $n = 0$.

2.2 Non-linear evolution

We evolve our initial conditions into the non-linear regime using a particle-mesh (PM) N -body code written by Changbom Park. This code employs a staggered-mesh technique (Melott 1986) to achieve higher force resolution than a conventional PM code. The code is thoroughly described by Park (1990), and it has been tested against analytic solutions and other N -body codes (Park 1990; Weinberg *et al.*, in preparation, hereafter W+). The W+ tests show that this PM code reproduces the results of high-resolution P³M (*e.g.*, Efstathiou *et al.* 1985) and tree (*e.g.*, Hernquist, Bouchet, & Suto 1991) N -body codes down to the limit of its force resolution, about 1-2 mesh cells. The chief advantage of the PM method is speed – P³M or tree code simulations with the same mass resolution as our PM experiments would have taken several times longer to perform.

PM simulations require a trade-off between force resolution and the size of the simulation volume, since the dimensions of the computational grid are usually limited by memory and cpu constraints. We need a large simulation volume for the reasons discussed in §1, but because the VPF is insensitive to small-scale clustering we can get away with relatively low force resolution. Our simulations of ‘ Γ ’ models (those with a CDM-like power spectrum) use 100^3 particles on a 200^3 density-potential mesh to represent a $300 h^{-1}$ Mpc, comoving, periodic cube. For simulations with power-law initial spectra (about whose realism we are somewhat less concerned), we use 64^3 particles on a 128^3 mesh, and a $192 h^{-1}$ Mpc simulation cube. In all cases the mesh scale is $\sim 1.5 h^{-1}$ Mpc. We have used trial runs of smaller volumes to confirm that we obtain the same VPF with a force resolution (mesh scale) of 0.5, 0.75, 1.0, and $1.5 h^{-1}$ Mpc. We have also checked that the VPF is unaffected by using 1 particle per 8 cells during dynamical evolution instead of 1 particle per cell; the sparser particle grid allows us to use a larger simulation volume with a fixed computer memory. Although we use a 200^3 mesh (or 128^3 for power-law models) to compute forces during non-linear evolution, we set up our initial conditions using a 100^3 (or 64^3) density field so that we do not alias high frequency power into our initial particle distributions.

We use the Zel’dovich approximation to turn our initial density fields into initial positions and growing-mode velocities for our N particles (see Doroshkevich *et al.* 1980; Efstathiou *et al.* 1985). All our simulations begin at a redshift z_{init} and advance to the present epoch in z_{init} timesteps, which are equally spaced in the expansion factor $a(t)$. We use $z_{\text{init}} = 31$ for the ‘ Γ ’ model simulations, and $z_{\text{init}} = 24$ for the power-law simulations. Again, we have used trial runs on smaller volumes to check our choices of initial redshift and timestep. Doubling z_{init} or the number of timesteps would not alter the VPF of our simulations. Halving z_{init} or the number of timesteps would have a tiny impact in a few cases. We computed two realizations of each of the ‘ Γ ’ models, and four realizations of each of the power-law models.

2.3 Normalization

The amplitude of primordial density fluctuations cannot presently be calculated *a priori* from theory, and we treat it as a free parameter of our models. The choice of amplitude is important, since larger amplitude perturbations produce stronger clustering and larger voids. [In an $\Omega = 1$ model, choosing the amplitude normalization is equivalent to choosing the time in an evolving N -body simulation that corresponds to the present, and voids grow as a simulation evolves.] We normalize our models by making them fit an observational constraint, *viz.*, the rms fluctuation of galaxy counts in spheres of radius $8 h^{-1}$ Mpc at the present epoch t_0 . Estimates of the galaxy correlation function (*e.g.*, Davis & Peebles 1983) imply that this quantity is close to unity, *i.e.*, $\sigma_{8,\text{gal}}(t_0) \simeq 1$. This condition and the relation $\sigma_{8,\text{gal}} = b \sigma_{8,\text{mass}}$ imply that for our unbiased models – where

galaxies are assumed to trace the mass distribution ($b = 1$) – the present epoch can be identified as the time when the rms mass fluctuation in spheres of radius $8 h^{-1}$ Mpc equals one, *i.e.*, $\sigma_{8,\text{mass}} \simeq 1$.

In the ‘ Γ ’ models, the quantity $\sigma_{8,\text{mass}}$ evolves at close to its linear theory rate throughout our simulations. We therefore normalize our initial conditions so that they have $\sigma_8 = 1$ if extrapolated to $z = 0$ by linear theory. For some of the power-law models, particularly $n = 0$, the growth of σ_8 departs significantly from linear theory, as discussed by WC. We adopt the normalization amplitudes computed by WC (see their table 1), so that the non-linear values of σ_8 in the simulations are equal to one at $z = 0$. The corresponding linear theory amplitudes are $\sigma_8 = 1.48$, 1.03 , and 0.95 for $n = 0$, -1 , and -2 , respectively.

The VPF is a sensitive function of the mean galaxy density n , or equivalently, of the characteristic inter-galaxy separation $\bar{d} \equiv n^{-1/3}$ (increasing the separation of galaxies increases the sizes of voids). It is therefore important that our simulated data have the same density as the real data to which they are being compared. Once we evolve our normalized initial conditions to $z = 0$, we therefore require that our simulated galaxies have the characteristic separation $\bar{d} = 4.5 h^{-1}$ Mpc of VGH’s densest sample. To create an unbiased galaxy population with $\bar{d} = 4.5 h^{-1}$ Mpc, we randomly sample the particles in our final mass distribution to this density.

The normalization scheme discussed so far ignores the possibility of biased galaxy formation. To create biased simulations with bias factors $b = 1.5$, 2 , and 3 , we reduce the amplitudes of the initial mass fluctuations by a factor of b , and evolve them to $z = 0$ by an N -body simulation as before. We then select a biased (instead of random) subset of the particles to represent galaxies. Our density biasing and peaks biasing prescriptions each contain an adjustable parameter that controls the strength of clustering in the biased particle subset. We select this parameter so that $\sigma_{8,\text{gal}} = 1$. To the extent that $\sigma_{8,\text{mass}}$ follows linear theory, the ratio of rms galaxy fluctuations to rms mass fluctuations at the final epoch on the scale of $8 h^{-1}$ Mpc is b .

Instead of trying a variety of bias factors, we could have normalized the mass fluctuations in our models by matching the amplitude of temperature fluctuations in the cosmic microwave background (CMB), as observed by COBE (Smoot *et al.* 1992). We did not take this approach, for several reasons. First, predicting CMB fluctuations on the large angular scales probed by COBE would require us to extrapolate our model power spectra to wavelengths much larger than those that influence the formation of voids. This extrapolation would make little physical sense for power-law spectra, and even for the ‘ Γ ’ models the resulting normalization would be unduly sensitive to our precise choice of parameters. For example, lowering Γ from 0.25 to 0.2 at fixed σ_8 would have a negligible impact on void sizes, but it would significantly alter the relation between σ_8 and COBE-scale CMB fluctuations. Second, there are still significant random and systematic uncertainties in the COBE fluctuation amplitude. Finally, it is possible that some fraction of the COBE signal arises from tensor mode (gravity wave) fluctuations instead of the scalar mode fluctuations that correspond to density perturbations (Davis *et al.* 1992; Liddle & Lyth 1992; Lidsey & Coles 1992; Lucchin *et al.* 1992; Salopek 1992; Souradeep & Sahni 1992). For what it is worth, EBW find that the best-fit COBE amplitude implies $\sigma_8 \approx 1.1$, 0.5 , and 1.25 respectively for our spatially flat models with $(\Gamma, \Omega_0) = (0.5, 1)$, $(0.25, 1)$, and $(0.25, 0.3)$, assuming a truly scale-invariant primeval spectrum and no contribution from gravity waves.

2.4 Biasing Schemes

In principle, the existence and nature of biased galaxy formation should be a prediction of a theoretical model, not an input. A complete theory specifies both the initial conditions and the important physical processes for structure formation, and from these one should be able to compute

where the galaxies form and how they cluster relative to the mass. In practice, the necessary computations are very difficult, and there are uncertainties in the appropriate treatment of gas physics and star formation. Most large-scale structure simulations therefore rely on simplified prescriptions for identifying “galaxy” particles. Simplest of all is the assumption that galaxies trace the mass, which is the rule we adopt in our unbiased models. We also consider two different prescriptions for biased galaxy formation, one that identifies galaxies with particles that lie above a sharp threshold density in the final conditions, and one that associates galaxies statistically with high peaks of the initial density field. For the $b = 1.5$ CDM model we also try a somewhat more sophisticated approach, applying a galaxy identification algorithm that has been “calibrated” from cosmological simulations with hydrodynamics.

This last scheme is based on the simulation of Cen & Ostriker (1993, hereafter CO; see also Cen & Ostriker 1992), and we refer to it as ‘C/O biasing.’ CO simulate the standard CDM model ($\Omega = 1$, $\Gamma = 0.5$) with $\sigma_{8,\text{mass}} = 0.77$ and a simulation volume $80 h^{-1}$ Mpc on a side. Their simulations include dissipation and star formation in a baryonic component, and they apply a percolation algorithm to group “star” particles into “galaxies” at $z = 0$. In their analysis, they fit the relation between the smoothed galaxy number density n_{gal} and the smoothed mass density ρ_{mass} to the functional form

$$\log(n_{\text{gal}}/\bar{n}_{\text{gal}}) = A + B \log(\rho_{\text{mass}}/\bar{\rho}_{\text{mass}}) + C [\log(\rho_{\text{mass}}/\bar{\rho}_{\text{mass}})]^2. \quad (1)$$

CO list values of A , B , and C for Gaussian smoothing filters of various radii. We want to select particles from an N -body simulation, and for this purpose it is easier to use cubic cells rather than Gaussian filters, since every particle is a member of a distinct cell. R. Cen has kindly computed the parameters of equation (1) for us using $2 h^{-1}$ Mpc cubic cells. To select biased particles, we compute the final mass density field on a 150^3 grid and apply equation (1) to compute the galaxy density in each cell, using a mean galaxy density \bar{n}_{gal} equal to the density of VGH’s densest observational sample (for which $\bar{d} \equiv \bar{n}_{\text{gal}}^{-1/3} = 4.5 h^{-1}$ Mpc). We then select particles from cell \vec{x} with probability $p = n_{\text{gal}}(\vec{x})/n_{\text{p}}(\vec{x})$, where $n_{\text{p}}(\vec{x})$ is the particle number density in the cell. We use cloud-in-cell weighting to compute the density field and to assign selection probabilities to particles. For $2 h^{-1}$ Mpc cells, Cen finds $B = 1.9$ and $C = -0.20$; the value of A is determined by the requirement that the mean density of selected particles equal the desired mean galaxy density \bar{n}_{gal} . As a check, we have computed galaxy and mass density fields from our biased and unbiased particle distributions, with Gaussian smoothing filters of radius 3 and $5 h^{-1}$ Mpc. The relation between smoothed galaxy density and smoothed mass density is then close to equation (1), as evaluated with the values of B and C that CO report for these smoothing radii. This agreement confirms that our particle selection scheme provides a reasonable representation of CO’s biasing results.

Of the three biasing schemes that we use, the C/O scheme has the clearest physical motivation. However, one should bear in mind that the CO simulations have a resolution of only $\sim 400 h^{-1}$ kpc, which may not be adequate for identifying galaxies reliably. The simulations of Katz, Hernquist & Weinberg (1992) and Evrard, Summers & Davis (1993), which model the baryon component using smoothed-particle hydrodynamics, have much higher spatial resolution in galaxy-forming regions, but the simulation volumes are not large enough to allow a meaningful definition of a biasing relation like equation (1). For now, we take CO’s result as a plausible illustration of the sort of biasing relation that can be derived from cosmological simulations with gas dynamics and galaxy formation. Since the C/O relation is derived specifically for standard CDM with $b \approx 1.5$, we apply it only to this particular model. Changing the normalization, the shape of the power spectrum, or the value of Ω would alter the collapse times of galaxy-scale perturbations, so it is not at all obvious how the properties of biasing would respond to these changes.

Our ‘density biasing’ scheme is similar to the C/O scheme discussed above, but instead of the non-linear function (1), we simply adopt a sharp threshold — galaxies form with equal probability where the smoothed mass density exceeds some value, and they do not form at all where the mass density is below this value. Specifically, we create a final density field from the $z = 0$ distribution of mass points, and smooth it with a Gaussian filter of radius R_s . We set $R_s = 2.25 h^{-1}$ Mpc for consistency with the peaks biasing procedure described below. We then compute the smoothed density at the final location of each particle, and select some fraction f_b of particles that have the highest local densities. As this fraction diminishes, the corresponding subset of particles becomes more and more biased towards the densest regions of the simulation. We randomly sample this biased subset to the desired inter-galaxy separation $\bar{d} = 4.5 h^{-1}$ Mpc, and we identify the resultant population of points as the ‘galaxies’ of interest. The value of f_b is chosen so $\sigma_{8,\text{gal}}(t_0)$ for this biased and sampled subset matches that of the corresponding unbiased simulation. This sharp threshold in final density is the biasing scheme used by EEGS and by WC.

The ‘peaks biasing’ scheme, which has been widely used in previous studies of CDM models, is simple in conception but complicated to implement in practice. One might naturally expect that peaks of the primordial density field would become the first sites of non-linear gravitational collapse (though Katz, Quinn & Gelb [1993] find a rather poor correspondence between galaxy-scale peaks of the initial density field and collapsed dark halos in N -body simulations). The assumption behind peaks biasing is that bright galaxies form only at galaxy-scale peaks of the initial density field that lie above some global threshold $\nu_t \equiv \delta_{\text{mass}}/\sigma_{\text{mass}} > 1$. Lower height peaks are assumed to form underluminous galaxies or structures not recognized as galaxies at all. A number of authors have discussed physical mechanisms that might lead to such a thresholding effect, among them Rees (1985), Silk (1985), Dekel & Silk (1986), White *et al.* (1987), Kaiser (1988), and Cole & Kaiser (1989).

Kaiser (1984) showed that the high peaks of a Gaussian density field cluster more strongly than the underlying mass distribution, and he suggested that this phenomenon might explain the high amplitude of the observed cluster-cluster correlation function. BBKS applied the same idea to galaxy formation, and they computed many of the statistical and clustering properties of peaks of Gaussian fields. The strength of biasing between the high peaks and the underlying density field depends on the importance of long wavelength perturbations in the initial conditions. Long wavelength perturbations modulate the background density, and they therefore alter the local effective threshold height, *i.e.*, the relative ease with which a peak relative to the *local* background can rise above a *global* threshold. In a Gaussian random field, the number density of rare peaks is a strong function of peak height, so small changes in the effective threshold height can lead to large changes in the local number density of peaks above a global threshold. If the primordial fluctuations have appreciable large-scale power (as in CDM), then the high peaks occur preferentially in regions of high background density. Bright galaxies that form around these high peaks are ‘born’ clustered, so they provide biased tracers of the underlying mass distribution.

When applied to a given mass distribution, the peaks biasing scheme has two free parameters. The first is the smoothing scale for defining galaxy peaks, R_g (in our case, R_g is the radius of a Gaussian window function). This radius defines the characteristic physical size of the peaks, so it should correspond approximately to the mass scale of a typical galaxy. Since the precise relation between the smoothing scale and the collapsed mass is uncertain, we have a fair amount of freedom in our choice of R_g . The second free parameter is the peak threshold height ν_t — this measures the ‘difficulty’ of galaxy formation. The values of R_g and ν_t can be fixed by requiring that the biased model with which they are associated fit two observational numbers, usually taken to be the galaxy number density (or the associated characteristic separation $\bar{d} \equiv n^{-1/3}$, in our case $4.5 h^{-1}$ Mpc) and the rms amplitude of galaxy count fluctuations on some scale (in our case, $\sigma_{8,\text{gal}} \simeq 1$).

Our initial conditions do not resolve galaxy scales, so we implement peaks biasing via the peak-background split approximation, which allows one to identify particles with galaxy-scale peaks in a statistical manner, given the density field smoothed over a larger scale (BBKS; see also Park 1991). The approximation relies on the fact that δ_g – the full initial density field smoothed on the galaxy scale R_g – has the same power spectrum and hence the same statistical properties as the field $\delta_b + \delta_p$, where δ_b is a field with the same underlying power spectrum as δ_g but smoothed on a larger, background scale R_b , and δ_p is a ‘peaks’ field whose power spectrum is that of δ_g minus that of δ_b . One can therefore estimate the local density of peaks in δ_g above a global threshold ν_t as the number of peaks in δ_p above a local effective threshold, whose value is modulated by the background field δ_b . The use of the peak-background split approximation introduces a third parameter into our biasing prescription, the background smoothing length R_b . Given our choice of R_g (see below), we adopt a Gaussian window radius $R_b = 2.25h^{-1}$ Mpc. This value ensures that $3 < R_b/R_g < 5$, as required for best results in the peak-background split approximation (BBKS, Park 1991). With this condition satisfied, our results should not be sensitive to the exact value of R_b .

In all our implementations of peaks biasing, we use equation (6.35) of BBKS to calculate the expected local number density $n_{\text{pk}}(\delta_b)$ of galaxy-scale peaks above ν_t , as a function of the background field height δ_b . We identify a mass particle that lies in a given cell \vec{x} of the initial conditions as a ‘galaxy’ with a probability equal to $A \cdot V \cdot n_{\text{pk}}[\delta_b(\vec{x})]$, where V is the cell volume and A is a constant of proportionality discussed below. At a mechanical level, this operation is quite similar to that in density biasing or C/O biasing, except that we select particles based on the initial rather than the final density field, and we use the rather complicated relation between galaxy and mass density implied by the peaks formulae instead of a sharp threshold function or the C/O relation. In a strict implementation of peaks biasing, the proportionality constant A is equal to one, and in this case the biasing operation has a clear physical interpretation: the selected particles correspond, statistically, to galaxy-scale peaks of the initial density field. To compare our models with VGH’s brighter, less dense samples (those with $\bar{d} > 4.5 h^{-1}\text{Mpc}$), we randomly sample our biased particle distributions to the desired number density. By so doing, we make the implicit assumption that galaxy biasing is independent of luminosity, at least for galaxies brighter than those of VGH’s densest sample (absolute magnitudes $M < -18.5$). We could instead have identified brighter galaxies with higher, rarer peaks, which are more strongly clustered. The first assumption makes physical sense if random factors independent of peak height determine a galaxy’s final luminosity.

At a fixed value of R_g , the strength of biasing is quite sensitive to the threshold ν_t . One might therefore think that the peaks biasing prescription could yield any bias factor of interest with an appropriate choice of parameters, in particular that for any value $1/3 \lesssim \sigma_{8,\text{mass}} \lesssim 1$ one could find values of the peak parameters ν_t and R_g that would yield $\sigma_{8,\text{gal}} = 1$. However, there is a second observational constraint to be matched, in our case the characteristic separation $\bar{d} = 4.5 h^{-1}\text{Mpc}$. We find that with the galaxy density or separation imposed as a constraint, the strict peaks biasing prescription (with the proportionality constant $A = 1$) can yield only a rather narrow range of bias factors for a given mass fluctuation spectrum.

This limitation arises because R_g and ν_t both affect \bar{d} and $\sigma_{8,\text{gal}}$ in the same sense. If the smoothing length R_g is fixed, then increasing ν_t increases \bar{d} (since higher peaks are rarer), and it increases $\sigma_{8,\text{gal}}$ (since higher peaks are more strongly clustered). If the threshold height ν_t is fixed, then increasing R_g increases \bar{d} (since it reduces the choppiness of the density field and thus increases the space between peaks), and it increases $\sigma_{8,\text{gal}}$ for a reason that is readily appreciated in terms of the peak-background split. Raising R_g reduces the amplitude of fluctuations associated with the ‘peaks’ field δ_p , so the large-scale waves have more influence in raising local peaks above the

global threshold, making the global peaks more strongly biased towards regions of high background density (see BBKS equation 6.35). With the strict peaks biasing scheme, raising ν_t to get a higher bias factor also raises \bar{d} . To keep \bar{d} fixed (as we require for our comparison to the VGH data), R_g must be correspondingly lowered, but this also lowers b . These two effects on b nearly cancel in our models, so over the plausible range of peaks parameters the bias factor in a given model is nearly constant.

For our $\Gamma = 0.5$ and $\Gamma = 0.25$ models, the strict peaks biasing prescription works well for $\sigma_{8,\text{mass}} = 1/1.5$ ($b = 1.5$). The peak parameters $R_g = 0.57 h^{-1}\text{Mpc}$ and either $\nu_t = 1.8$ (for $\Gamma = 0.5$) or $\nu_t = 1.6$ (for $\Gamma = 0.25$) yield $\sigma_{8,\text{gal}} \approx 1$ and $\bar{d} \approx 4.5 h^{-1} \text{Mpc}$, as desired. However, when $\sigma_{8,\text{mass}} = 1/2$ or $1/3$, we cannot find peak parameters that produce a strong enough bias, *i.e.*, if we require $\bar{d} = 4.5 h^{-1}\text{Mpc}$, then no choice of peak parameters gives $\sigma_{8,\text{gal}} = 1$. We therefore adopt a relaxed version of the peaks prescription that can produce higher bias factors. To avoid the cancellation effect described above, we fix R_g at $0.57 h^{-1}\text{Mpc}$, and we vary ν_t to obtain the desired bias factor (*i.e.*, to obtain $\sigma_{8,\text{gal}} = 1$). We then vary the proportionality constant A in order to achieve the desired characteristic separation, $\bar{d} = 4.5 h^{-1}\text{Mpc}$. For the $b = 2$ and $b = 3$ models we require $A > 1$, making the abundance of selected galaxy particles larger than the abundance of peaks. Although our biasing formula is based on the peaks approach, in these cases there is no direct correspondence between the selected particles and peaks. This is somewhat unsatisfying, but since the peaks model (and any other biasing model) is at best an approximation of physical processes whose details are not well understood, it seems sensible to loosen the model a bit when necessary. For $b = 2$ the values of \bar{d} that we would obtain with $A = 1$ are $\sim 6 - 7 h^{-1}\text{Mpc}$, so for the two brightest VGH samples, which have $\bar{d} = 7.4$ and $10.9 h^{-1}\text{Mpc}$ respectively, we can still identify the simulations' galaxy particles with a subset of the high peaks.

3. Results

3.1 Visual Appearance of the Models

Figure 2 displays representative Cartesian slices from the final-time particle distributions of our models. Each panel displays a $15 h^{-1}\text{Mpc}$ thick slice through the simulation cube, with the galaxy population sampled to the characteristic separation $\bar{d} = 5.6 h^{-1} \text{Mpc}$ of VGH's $M_{\text{lim}} = -19$ samples. Axis scales are marked in $h^{-1}\text{Mpc}$. Figure 2a displays slices from unbiased and density-biased power-law models (simulation cubes $192 h^{-1}\text{Mpc}$ on a side). Its three rows show $n = 0$, -1 , and -2 models from top to bottom, and its four columns show $b = 1, 1.5, 2,$ and 3 models from left to right. Figures 2b and 2c display galaxies from the ‘ Γ ’ models (simulation cubes $300 h^{-1} \text{Mpc}$ on a side). The columns have the same b associations as Figure 2a, but Figures 2b and 2c display peaks-biased and density-biased models, respectively. The three rows of these figures are associated with $(\Gamma, \Omega_0, \lambda_0) = (0.5, 1, 0), (0.25, 1, 0),$ and $(0.25, 0.3, 0.7)$ models, from top to bottom. Throughout Figure 2 the largest rounded voids are much smaller than the panels, indicating that our simulation cubes are indeed large enough to allow a fair measure of voids for the range of models that we consider.

The initial conditions of all the models in Figure 2a were generated using the same random phases, as were all the models in Figures 2b and 2c. Thus within Figure 2a and throughout Figures 2b and 2c, recognizable structures tend to form at similar locations in different slices. Each model nonetheless produces distinctive structure, and one can notice several trends. Comparing panels within a given row of Figure 2, as one moves from left to right the low density regions become emptier, and the high density regions become more diffuse. Thus biasing has two basic effects on

Figure 2a

Figure 2a is a 0.5 Mbyte postscript file

Figures 2b and 2c are 1.2 Mbyte postscript files

You may obtain these files by request from

dhw@guinness.ias.edu

Figure 2 — Slices through the simulated galaxy distributions at $z = 0$. In every panel the rms galaxy fluctuation in spheres of radius $8 h^{-1}$ Mpc is unity, the characteristic inter-galaxy separation is $\bar{d} = 5.6 h^{-1}$ Mpc, and the thickness of the Cartesian slice is $15 h^{-1}$ Mpc. For all three plots, the four columns from left to right show models with bias factors $b = 1, 1.5, 2,$ and 3 . (a) Unbiased and density-biased power-law models, with $n = 0, -1,$ and -2 in the rows from top to bottom. (b) Unbiased and peaks-biased models, with $(\Gamma, \Omega_0, \lambda_0) = (0.5, 1, 0), (0.25, 1, 0),$ and $(0.25, 0.3, 0.7)$ from top to bottom. (c) Same as (b), but with peaks-biased slices replaced by corresponding density-biased slices.

spatial structure: it turns low density regions into completely empty voids, and it reduces the non-linearity of high density regions. The first effect arises because biasing suppresses galaxy formation in low density regions. The second effect arises because the mass fluctuations in our biased models are smaller, and they are therefore less efficient at inducing gravitational collapse. Recall that all of the models pictured in Figure 2 have the same rms fluctuation in galaxy counts at $8 h^{-1}$ Mpc.

Comparing corresponding $b \geq 1.5$ panels from Figures 2b and 2c, it is clear that the empty voids in density-biased models are larger than their peaks-biased counterparts. [Correspondingly, we will find that the density-biased VPFs in our simulations are always higher than their peaks-biased counterparts.] This is to be expected, since there is no more efficient way of creating voids than by ‘density biasing’, *i.e.*, by completely eliminating all particles from low density regions of the final conditions. Peaks biasing, on the other hand, permits occasional galaxy formation in low density regions. The rounded, ‘bubble-like’ voids in many of the biased models are reminiscent of features in wedge diagrams from the CfA2 redshift survey (de Lapparent *et al.* 1986; 1991) or the

Figure 2b

Figure 2 — *continued*

Perseus-Pisces redshift survey (Haynes & Giovanelli 1986; 1988). However, one should be cautious in drawing conclusions from visual comparisons, because properties of real-space, Cartesian slices like those in Figure 2 can be quite different from those of the redshift-space, magnitude-limited, declination wedges that are often used to display redshift survey results.

Our spectra are normalized to have the same amplitude at $\sim 8 h^{-1}$ Mpc. In the power-law models of Figure 2a, the models with steeper spectra (lower n) have more power on larger scales and less power on smaller scales. Both of these properties manifest themselves clearly in the slices. Models with steeper spectra develop coherent features that can be traced over a larger fraction of the simulation cube, and models with shallower spectra develop final structure that is clumpier on small scales. The ‘ Γ ’ models of Figures 2b and 2c exhibit less variation in spatial structure than the power-law models because the differences in the initial power spectra are themselves much smaller. However, comparing the $\Omega_0 = 1$ models in Figures 2b and 2c, $\Gamma = 0.5$ in the top rows and $\Gamma = 0.25$ in the middle rows, one sees that void sizes increase slightly among biased models as Γ is lowered. It is also possible to detect smoother, more coherent filaments in the models with more large-scale power (lower Γ). Comparing the middle and bottom rows in the same figures shows the effect of lowering Ω_0 while keeping the initial power spectrum fixed. Lowering Ω_0 reduces peculiar velocities on all scales because there is less mass available to attract condensations away from pure Hubble flow. However, Ω_0 has little effect on final spatial structure if fluctuations are normalized

Figure 2c

Figure 2 — *continued*

to the final epoch — at the level of the Zel’dovich approximation or the adhesion approximation it has no effect at all (see Weinberg & Gunn 1990). Some systematic differences between high- Ω_0 and low- Ω_0 models appear in the fully non-linear regime (see WC), but at the limited resolution of these slice plots, the differences are essentially undetectable. In terms of visual appearance, the effects of biasing easily outweigh the effects of Ω_0 or of the initial power spectrum.

3.2 Measuring the VPF

Our principal measure of the size and frequency of voids is the void probability function, the probability $P_0(R)$ that a randomly placed sphere of radius R contains no galaxies. We also employ a related statistic, the probability $P_{80}(R)$ that the average density in a randomly placed sphere is more than 80% below the global mean density. We also call $P_{80}(R)$ the underdense region probability function, or UPF. White (1979) discussed the relation between count probability statistics, including the VPF, and correlation function statistics. Following White’s original suggestion, many later studies of the VPF adopted the ‘scaled’ variables $\chi(\bar{N}\bar{\xi}) \equiv -\ln[P_0(R)]/\bar{N}$, where \bar{N} and $\bar{\xi}$ are respectively the mean number of galaxies and the mean value of the two-point correlation function in spheres of radius R (*e.g.*, Fry 1986, Maurogordato & Lachièze-Rey 1987, Fry *et al.* 1989; Lachièze-Rey, da Costa & Maurogordato 1992). This choice of variables allows one to test the so-called

hierarchical hypothesis, the assumption that all higher-order correlation functions can be expressed as sums of pairwise products of two-point correlation functions. However, the introduction of $\bar{\xi}$ into the scaled radius variable obscures the relation between the scaled VPF, $\chi(\bar{N}\bar{\xi})$, and the actual sizes of voids. Since we are interested in the frequency of large voids rather than the hierarchical hypothesis, we have decided to stick with the simpler representation $P_0(R)$.

VGH present VPFs for volume-limited subsets of the CfA redshift survey with the absolute magnitude limits $M_{\text{lim}} = -18.5, -19.0, -19.5,$ and -20.0 (for $h = 1$). The characteristic separations corresponding to these four limits, derived from the galaxy luminosity function, are $\bar{d} = 4.5, 5.6, 7.4,$ and $10.9 h^{-1}$ Mpc, respectively. The procedures described in §2 create simulated galaxy samples with a final-time separation of $\bar{d} = 4.5 h^{-1}$ Mpc. To compare our predictions with all the data of VGH, we subsequently sample this population to separations of $\bar{d} = 5.6, 7.4,$ and $10.9 h^{-1}$ Mpc. As mentioned in §2, because we randomly sample to compare to brighter subsets of the VGH data, our models implicitly assume that biasing (if any) is independent of galaxy luminosity for $M < -18.5$.

For our power-law models, we present VPF results only in real space, ignoring possible distortions from peculiar velocities. Measuring the VPF in real space is simple because our simulation volume is triply periodic. We choose 2000 random points throughout the simulation volume, and about each point we count the number of galaxies in concentric spheres of radius 1, 2, 3, \dots $R_{\text{max}} h^{-1}$ Mpc, including particles across a periodic boundary if necessary. We adopt $R_{\text{max}} = 35 h^{-1}$ Mpc, a radius by which $P_{80}(R)$ drops to zero in nearly all of our models. We set $P_0(R)$ equal to the number of empty spheres of radius R divided by the total number (2000) of spheres of radius R placed in the simulation volume. Similarly, we set $P_{80}(R)$ equal to the number of spheres that are at least 80% underdense, *i.e.*, that contain $N \leq 0.2(4\pi R^3/3\bar{d}^3)$ galaxies, divided by the total number of spheres of radius R . We have four independent simulations of each power-law model, and the VPFs that we plot are the average over these four runs.

For our ‘ Γ ’ models we evaluate the VPF and UPF in real space and in redshift space, *i.e.*, using the spherical coordinates (r, θ, ϕ) and $(r + v_r/H_0, \theta, \phi)$, where v_r is the radial peculiar velocity with respect to the observer, and H_0 is the Hubble constant. Adopting a v_r -dependent coordinate breaks the assumption of periodic boundary conditions, so our procedure for evaluating the VPF is more complicated than before. We want to measure the VPF in spherical rather than cubical samples because their redshift-space distortions are more likely to mimic those of a real observational sample — cubes have corners where the sample is unusually deep in the radial direction. We also want our samples to fill the simulation cube, so that we take full statistical advantage of the simulation volume. In each $300 h^{-1}$ Mpc simulation cube, therefore, we select 8 ‘observers’ located at the vertices of a smaller cube of side $L/2 = 150 h^{-1}$ Mpc. For each observer in turn, we shift particles (using the periodic boundaries) so that the observer lies at the center of the cube. We then move galaxies to redshift space and select a spherical sample containing all galaxies within a redshift distance $R_{\text{sample}} = 130 h^{-1}$ Mpc of the observer. We choose 500 random points within a sphere of radius $(R_{\text{sample}} - R_{\text{max}})$, and about each point we count galaxies in concentric spheres of radii 1, 2, 3, \dots $R_{\text{max}} h^{-1}$ Mpc. We define $P_0(R)$ and $P_{80}(R)$ as before, the number of empty or underdense spheres divided by the total number (500). We measure the real-space VPF and UPF in the same fashion, except that we omit the shift from real space to redshift space. All of a simulation’s cubical volume appears in at least one of the cube’s 8 samples, and most of it appears in more than one. There are two independent simulations of each ‘ Γ ’ model, and the results that appear in our figures are the average over all 16 ($= 2 \cdot 8$) relevant samples.

Figure 3 compares the real-space (solid line) and redshift-space (dotted line) VPFs of our unbiased, $(\Gamma, \Omega_0, \lambda_0) = (0.25, 1, 0)$ model. [Following WC, we use $\bar{d} = 5.6 h^{-1}$ Mpc here and in any other figures that display the VPF for only one value of \bar{d} .] At a given radius, the void probability

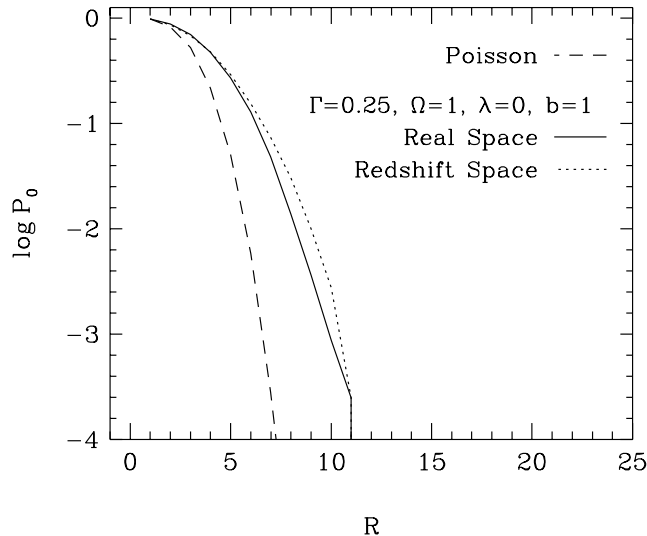


Figure 3 — The void probability function (VPF) in real space and redshift space. $P_0(R)$ is the probability that a randomly placed sphere of radius R (in h^{-1} Mpc) is empty of galaxies. Solid and dotted curves mark the real-space and redshift-space VPFs of our unbiased, $(\Gamma, \Omega_0, \lambda_0) = (0.25, 1, 0)$ model, with $\bar{d} = 5.6 h^{-1}$ Mpc. VPFs tend to be slightly higher in redshift space than in real space, probably because coherent outflows from low density regions shift galaxies outward from the positions that they occupy in physical space, stretching voids along the line-of-sight. The dashed curve shows the mean VPF for a Poisson distribution of particles with the same value of \bar{d} , $P_0(R) = \exp(-4\pi R^3/3\bar{d}^3)$. VPFs of the N -body models lie far above the Poisson VPF at large radii, as expected.

tends to be slightly higher in redshift space than in real space, probably because coherent outflows from low density regions move galaxies outward from the positions that they occupy in physical space, thereby increasing the sizes of voids along the line-of-sight (cf. figure 6 of Regös & Geller 1991). Although redshift-space VPFs in our simulations are almost always higher than their real-space counterparts, there are a few rare instances where they are lower – especially at large radii. Lower redshift-space VPFs can arise because velocity dispersions in groups and clusters scatter galaxies outward into regions that are empty in physical space. The differences between real-space and redshift-space VPFs are generally smaller than those in Figure 3 for models with smaller Ω_0 , larger Γ , larger b , or smaller \bar{d} . The trends with Ω_0 , Γ , and b are comprehensible, in that decreasing the mass density or the scale or amplitude of mass fluctuations leads directly to a decrease in large-scale peculiar velocities. The trend with \bar{d} probably occurs because the coherent outflows associated with voids are less evident at smaller separations.

The dashed curve in Figure 3 shows the VPF expected for a Poisson distribution of points with characteristic separation \bar{d} , $P_0(R) = \exp(-4\pi R^3/3\bar{d}^3)$. The model VPFs lie far above the Poisson VPF at large radii, as expected. Nonetheless, in Figure 3 and in the VPFs of all of our other models, P_0 drops to 10^{-4} at radii much smaller than $L/2 = 150 h^{-1}$ Mpc, confirming Figure 2’s indication that even our largest voids are much smaller than the simulation cube.

3.3 Dependence of the VPF on Model Parameters

3.3.1 Unbiased Models

Figure 4 illustrates the dependence of the VPF on the shape of the initial power spectrum for unbiased models. Solid, dotted, and dashed lines represent the real-space VPFs for our unbiased

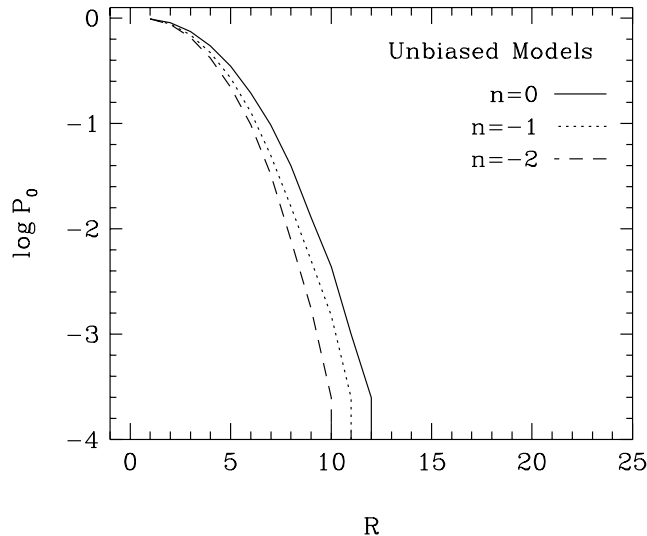


Figure 4 — Dependence of the VPF on the initial power spectrum, for unbiased models. Solid, dotted, and dashed lines show the real-space VPFs of unbiased power-law models with $\bar{d} = 5.6 h^{-1}\text{Mpc}$ and $n = 0, -1,$ and $-2,$ respectively. Increasing n leads to a modest increase in the VPF, but the trend is rather weak.

power-law models with $n = 0, -1,$ and $-2,$ respectively. The three curves are quite similar, showing that the VPF in unbiased models depends only weakly on the shape of the initial power spectrum. This insensitivity probably indicates that large empty regions grow from fluctuations near the $8 h^{-1}\text{Mpc}$ normalization scale, where all three models have the same rms amplitude. The VPFs in this figure nonetheless exhibit a systematic trend – as n is lowered, the VPF decreases slightly. The same trend is visible in the corresponding slice plots (column one of Figure 2a). WC also noted this effect among Gaussian models, and they cited two reasons for it. First, introducing small-scale power (increasing n) creates stronger negative fluctuations on small scales, and these lead directly to higher VPFs on those scales. Second, introducing small-scale power clumps galaxies on small scales, reducing the effective number of independent tracers; since the effective inter-particle density is thus lowered, the VPF goes up. Models with lower n have stronger fluctuations on large scales, but on these scales the fluctuation amplitude may be too low to clear out empty regions.

Figure 5 illustrates the dependence of the VPF (or lack thereof) on Ω_0 and λ_0 , for unbiased models. Five curves are plotted: solid, dotted, short-dashed, long-dashed, and dot-dashed lines for the real-space VPFs of unbiased, $\Gamma = 0.25$ models with the parameter combinations $(\Omega_0, \lambda_0) = (1, 0), (0.3, 0), (0.1, 0), (0.3, 0.7),$ and $(0.1, 0.9),$ respectively. Four of the curves lie so close to each other that they are indistinguishable on this plot. Only the $(\Omega_0, \lambda_0) = (0.1, 0)$ VPF stands slightly apart, and even in this case the differences in the tail of the VPF correspond to just one or two voids out of the 8000 randomly placed spheres. Figure 5 demonstrates that the real-space VPF is extremely insensitive to Ω_0 and λ_0 , if the power spectrum is held fixed. This insensitivity is not terribly surprising, since the final spatial structure is completely independent of Ω_0 and λ_0 at the level of the adhesion approximation, and one expects dynamical non-linearities to distinguish these models mainly in collapsed, virialized regions. In redshift space we find a mild dependence of the VPF on Ω_0 because the magnitude of peculiar velocity distortions depends on Ω_0 . However, we have already seen that the difference between real-space and redshift-space VPFs is small (Figure 3), and the differences between redshift-space VPFs with the same power spectrum but different values of Ω_0 are smaller still. At fixed Ω_0 , even the redshift-space VPF is insensitive to λ_0 because

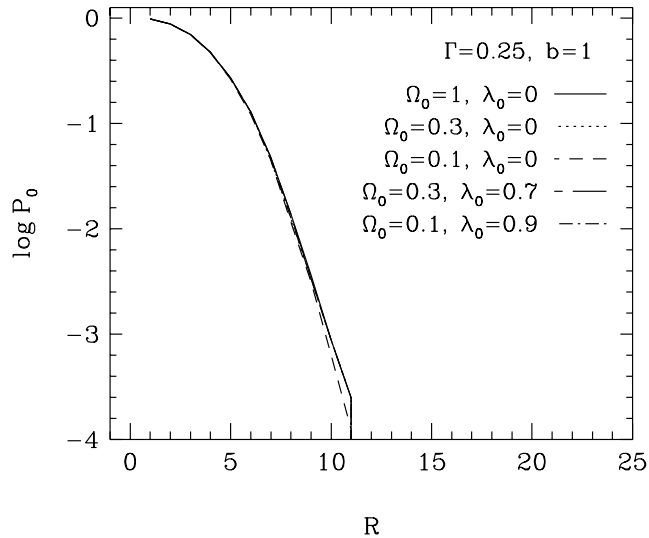


Figure 5 — Dependence of the VPF on Ω_0 (the cosmic density parameter) and λ_0 (the cosmological constant). Different line types show real-space, $\bar{d} = 5.6 h^{-1}$ Mpc VPFs of five unbiased, $\Gamma = 0.25$ models with five different combinations of Ω_0 and λ_0 , as labeled. Four of these VPFs are so similar that the curves are indistinguishable on this plot, and the fifth ($\Omega_0 = 0.1, \lambda_0 = 0$) is only marginally different. Within the parameter range shown here, Ω_0 and λ_0 have essentially no impact on the real-space VPF. The value of Ω_0 has a small effect on the redshift-space VPF, since it determines the amplitude of peculiar velocities.

peculiar velocities depend almost entirely on the density parameter rather than the cosmological constant.

3.3.2 Biased Models

Figure 6 illustrates the dependence of the VPF on the prescription adopted for biased galaxy formation, at a fixed bias factor $b = 1.5$ and a characteristic separation $\bar{d} = 5.6 h^{-1}$ Mpc. Solid, dashed, and dotted lines display real-space VPFs for standard CDM models ($\Gamma = 0.5, \Omega_0 = 1$), biased to $b = 1.5$ with peaks, density, and C/O biasing, respectively. Density biasing produces much higher VPFs than peaks biasing, as one would expect given the visual appearances of Figures 2b and 2c. This difference between the two biasing schemes holds for all of our models; it is even more pronounced for $\Gamma = 0.25$ (more large-scale power). Peaks biasing and C/O biasing, on the other hand, produce nearly identical VPFs. Although the difference between these schemes is somewhat larger for other values of \bar{d} , it is always very small.

Figure 7 illustrates the dependence of the VPF on the bias factor b , for density biasing (Figure 7a) and peaks biasing (Figure 7b). Figure 7a is designed for comparison with figure 4b of EEGS, which also shows real-space VPFs for spatially flat, low- Ω_0 , CDM models with different bias factors. Except for our choice of smoothing filter and our dilution to a fixed galaxy density, our density biasing scheme is the same as EEGS's biasing scheme. In Figure 7a, solid, dotted, short-dashed, and long-dashed lines represent real-space VPFs of our $(\Gamma, \Omega_0, \lambda_0) = (0.25, 0.3, 0.7)$ models, with biasing factors of $b = 1, 1.5, 2,$ and $3,$ respectively. In both EEGS's figure 4b and our Figure 7a, increasing the bias factor raises the VPF. However, the form of this trend differs dramatically in the two cases. In EEGS's figure, four successive increases in the bias factor produce a steady and uniform march of the VPF to appreciably higher values. EEGS's median void radii display a

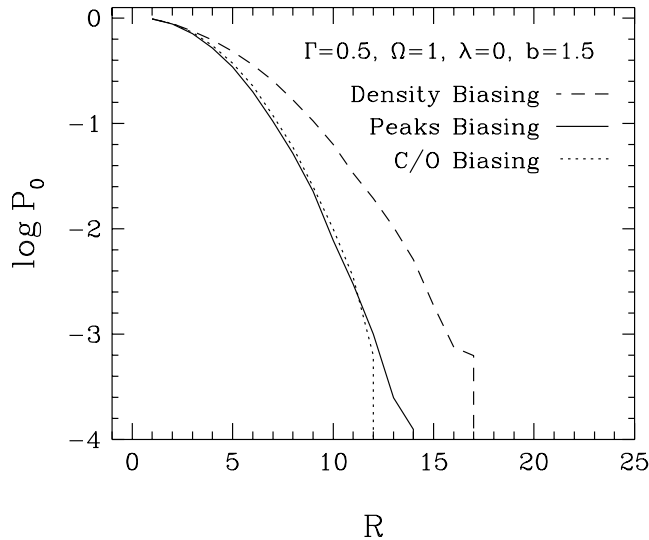


Figure 6 — Dependence of the VPF on the prescription for biased galaxy formation, at a fixed value of the bias factor b . Solid, dashed, and dotted lines show real-space, $\bar{d} = 5.6 h^{-1} \text{Mpc}$ VPFs for $b = 1.5$, ‘standard CDM’ models with peaks biasing, density biasing, and C/O biasing, respectively. Density biasing creates larger voids and a higher VPF than peaks biasing; the same trend holds for other models, other bias factors, and other values of \bar{d} . Peaks biasing and C/O biasing yield similar VPFs.

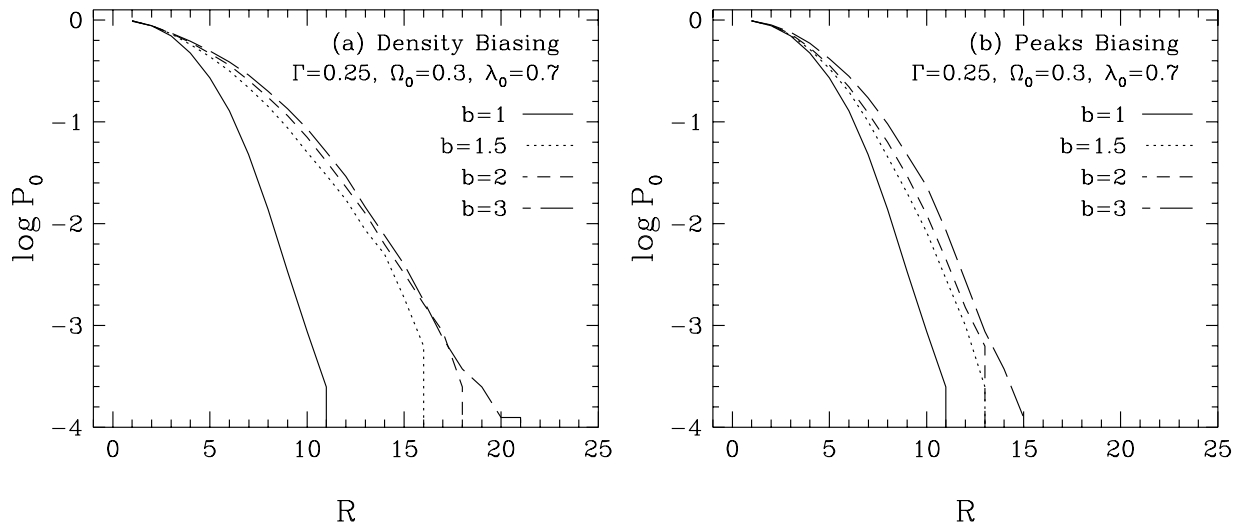


Figure 7 — Dependence of the VPF on the bias factor b . (a) Real-space, $\bar{d} = 5.6 h^{-1} \text{Mpc}$ VPFs for unbiased and density-biased models with $\Gamma = 0.25$, $\Omega_0 = 0.3$, and $\lambda_0 = 0.7$. The VPF jumps sharply between $b = 1$ and $b = 1.5$, but it increases only slowly over the entire remaining range, from $b = 1.5$ to $b = 3$. This behaviour contrasts with that in EEGS’s figure 4b, to which this plot can be compared. (b) Same as (a), but with density-biased VPFs replaced by corresponding peaks-biased VPFs. The latter are more like the corresponding unbiased VPF, though again there is a larger jump between $b = 1$ and $b = 1.5$ than between higher bias factors.

similar steady trend (see their table 2 and figure 6). It is exactly this systematic dependence which suggested that the VPF might be a sensitive indicator of biasing, and perhaps a statistical tool with which to determine the bias factor. In our Figure 7a, however, the VPF increases only weakly over the entire range $1.5 \leq b \leq 3$, despite a large increase between $b = 1$ and $b = 1.5$. This result is consistent with the visual appearance of successive columns in Figure 2c.

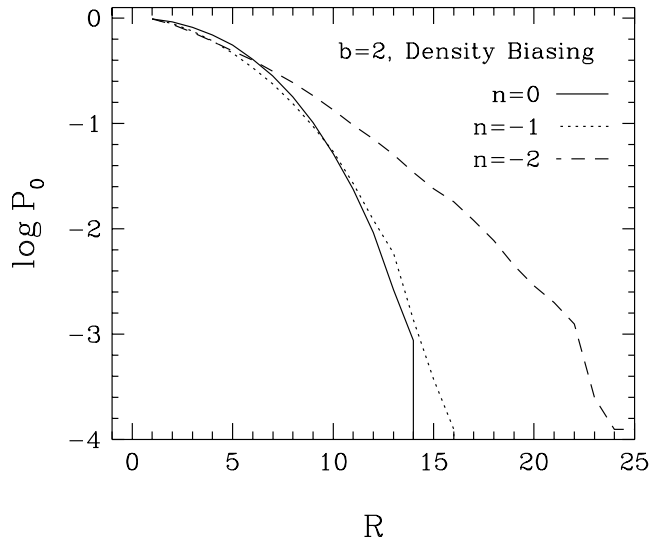


Figure 8 — Dependence of the VPF on the initial power spectrum, for biased models. Solid, dotted, and dashed lines show the real-space VPFs of density-biased power-law models with $\bar{d} = 5.6 h^{-1}\text{Mpc}$ and $n = 0, -1,$ and $-2,$ respectively. The first two VPFs are similar, but the biased $n = -2$ VPF is much higher, as biasing turns the $n = -2$ model’s large underdense regions into empty voids. The trend for biased models is quite different from that for unbiased models (cf. Figure 4).

There are many differences between our simulations and those of EEGS, but the difference in normalization procedure is probably the most important for explaining the different dependence on the bias factor. For their CDM models, EEGS take a fixed underlying mass distribution and choose successively more strongly biased subsets of the particles. Each increase in the bias factor yields a ‘galaxy’ population that is more strongly clustered in an rms sense, and it is not surprising that void sizes increase each time. However, at most one of these biased subsets can match the known rms fluctuation of galaxy counts as measured from the two-point correlation function. We adopt the observed rms fluctuation at $8 h^{-1}\text{Mpc}$ as a constraint on our ‘galaxy’ populations, so we accompany each increase in the bias factor with a corresponding decrease in the amplitude of the underlying mass fluctuations. The reduction in mass fluctuations counteracts the stronger biasing; in an rms sense the two effects cancel, by construction. Void sizes are sensitive to the efficiency of galaxy formation in low density regions, so some dependence of the VPF on b remains, but this dependence is strong only between $b = 1$ and $b = 1.5$.

Figure 7b illustrates the dependence of the VPF on the bias factor for the peaks biasing prescription. It is obtained by replacing the density-biased VPFs of Figure 7a with their peaks-biased counterparts. Once again the VPF is more sensitive to the difference between $b = 1$ (unbiased) and $b = 1.5$ than to the differences between $b = 1.5, 2,$ and 3 . However, the jump from $b = 1$ to $b = 1.5$ is much smaller than it is for density biasing, and the growth of the VPF with b is somewhat more steady.

Figure 8 illustrates the dependence of the VPF on the shape of the initial power spectrum for biased models (analogous to Figure 4 for unbiased models). Solid, dotted, and dashed lines display the real-space VPFs of our $b = 2,$ density-biased, power-law models with $n = 0, -1,$ and $-2,$ respectively. The $n = 0$ and $n = -1$ models have similar VPFs, but the $n = -2$ VPF is much higher. This behaviour contrasts with that in Figure 4, where all three models have similar VPFs and the $n = -2$ VPF is the lowest. WC found similar results for their biased models. While the

large-scale fluctuations in the $n = -2$ models are too weak to clear out empty voids by gravity alone, they do create large regions of low mass density, and biasing turns these regions into large, empty voids. We find the same trend — larger voids in biased models with more large-scale power — when comparing our $\Gamma = 0.5$ and $\Gamma = 0.25$ models, using either density biasing or peaks biasing. If one knew that galaxy formation were biased and one knew the specific nature of the bias, one could conceivably derive constraints on the primordial power spectrum from the VPF. However, given the uncertainties in the appropriate choice of biasing scheme, the VPF is probably not a useful diagnostic for $P(k)$. Voids tell us more about the relation between galaxies and mass than about the power spectrum of the mass distribution itself.

3.4 Basic Comparison to the Data

The Vogeley, Geller & Huchra (VGH) void probability data come from three magnitude-limited redshift surveys, ‘CfA1 North’, ‘CfA2 North’, and ‘CfA2 South’. The ‘CfA1 North’ survey consists of the northern part of the original CfA survey (Huchra *et al.* 1983), which is complete to a limiting apparent magnitude of 14.5, covers the range $\delta > 0^\circ$, $b^{II} > 40^\circ$, and contains 1833 galaxies. The ‘CfA2 North’ survey comes from the extension of the CfA survey to the limiting magnitude 15.5 (see Geller & Huchra 1989). It covers the range $8^h \leq \alpha \leq 17^h$, $26.5^\circ \leq \delta \leq 44.5^\circ$, and it contains 2556 galaxies. The ‘CfA2 South’ survey, also from the CfA extension, contains 2414 galaxies in the range $20^h \leq \alpha \leq 4^h$, $6^\circ \leq \delta \leq 36^\circ$. From each of these three surveys, VGH construct four volume-limited samples, the absolute magnitude of the faintest galaxies in these samples being $M_{\text{lim}} = -18.5, -19.0, -19.5,$ and -20 (for $h = 1$). The corresponding characteristic inter-galaxy separations, computed from the galaxy luminosity function, are $\bar{d} = 4.5, 5.6, 7.4,$ and $10.9 h^{-1}$ Mpc, respectively (see table 1 of VGH). These 12 volume-limited samples contain between 182 and 627 galaxies each, and they range in depth from 40 to $126 h^{-1}$ Mpc.

VGH computed VPFs for each of these 12 observational samples, and M. Vogeley has kindly provided these data to us in the form of computer files. Figure 9 compares the observational data to the predictions of our ‘T’ models. Open circles, asterisks, and open triangles display the VPFs measured from ‘CfA2 North’, ‘CfA2 South’, and ‘CfA1 North’, respectively. The four rows display VPFs for $\bar{d} = 4.5, 5.6, 7.4,$ and $10.9 h^{-1}$ Mpc samples, from top to bottom. The same 12 observational VPFs appear in each column of panels in Figure 9. The trend toward larger VPFs from top to bottom within a given column reflects the simple fact that increasing the characteristic inter-galaxy separation (decreasing the galaxy density) increases the sizes of empty voids. We have not attached error bars to the points of Figure 9; we will consider the effects of finite volume errors in the next section. For now we note simply that the three, largely independent observational samples give fairly consistent but not identical results.

Figures 9a, 9b, and 9c compare the VGH results to the redshift-space VPFs of our $(\Gamma, \Omega_0, \lambda_0) = (0.5, 1, 0), (0.25, 1, 0),$ and $(0.25, 0.3, 0.7)$ models, respectively. We do not include a comparison to the power-law models because they have less observational and theoretical motivation; WC show some comparisons between these models and the VGH data. In each panel of Figure 9, the solid, dotted, short-dashed, and long-dashed lines are associated with $b = 1, 1.5, 2,$ and $3,$ respectively. Left hand columns show results for peaks biasing, right hand columns for density biasing (the solid lines show unbiased models in each case). The dot-dashed lines in the right hand column of Figure 9a are associated with the C/O biasing scheme, for $b = 1.5$. Figure 9 exhibits many of the model trends seen in previous figures. For example, it confirms that density biasing produces significantly larger VPFs than peaks biasing, and that peaks biasing and C/O biasing produce nearly identical VPFs (cf. Figure 6). Figure 9 also confirms that the VPFs of unbiased models depend only weakly on $\Omega_0, \lambda_0,$ and the initial power spectrum (cf. Figures 4 and 5), and that increasing large-scale

Figure 9a

obtain by request (3 x 150 kb)

Figure 9 — Comparison between observed VPFs and the VPFs of our best-motivated theoretical models. Within each panel: (i) the circles, asterisks, and triangles are the observed, redshift-space VPFs calculated by Vogeley, Geller, and Huchra (1991; VGH) from volume-limited samples of the ‘CfA2 North’, ‘CfA2 South’, and ‘CfA1 North’ galaxy redshift surveys, respectively; (ii) the solid, dotted, short-dashed, and long-dashed lines are redshift-space VPFs calculated from our theoretical models with $b = 1, 1.5, 2,$ and $3,$ respectively. Within each of the three plots: (i) the four rows from top to bottom show VPFs for characteristic inter-galaxy separations $\bar{d} = 4.5, 5.6, 7.4,$ and $10.9 h^{-1}$ Mpc; (ii) the $b \geq 1.5$ lines in the left and right columns are associated with peaks biasing and density biasing, respectively. The dot-dashed lines in the right column of (a) are the redshift-space VPFs from our $b = 1.5,$ C/O-biased model. Figures (a), (b), and (c) show model VPFs for $(\Gamma, \Omega_0, \lambda_0) = (0.5, 1, 0), (0.25, 1, 0),$ and $(0.25, 0.3, 0.7),$ respectively. These VPFs exhibit many of the model-dependent trends discussed earlier. Unbiased, peaks-biased, and C/O-biased models generally reproduce the VGH data fairly well, while density-biased models tend to create an excess of large voids.

Figure 9b

Figure 9 — *continued*

power can substantially increase density-biased VPFs (cf. Figure 8) – as Γ is lowered, Figure 9’s density-biased VPFs increase appreciably. This effect is also present, though less pronounced, among peaks-biased models. Finally, within a given panel of Figure 9 the difference between $b = 1$ and $b \geq 1.5$ VPFs is often much larger than the difference among $b \geq 1.5$ VPFs (cf. Figure 7). This effect is especially strong among density-biased models and models with more large-scale power, because they are least like their unbiased counterparts. The effect is weaker for larger values of \bar{d} because increasing \bar{d} raises unbiased VPFs relative to their biased counterparts. The impact of increasing \bar{d} is evidently greater when a smaller fraction of the total volume is already empty (*i.e.*, in unbiased models).

Figure 9c

Figure 9 — *continued*

Turning to a comparison with the data, it is clear that the density-biased models of Figure 9 generally tend to overproduce voids. This tendency weakens (and occasionally reverses) as \bar{d} increases (*i.e.*, as the observed VPFs go up), or as large-scale power or Ω_0 decrease (so that model VPFs go down). However, all of our density-biased models match the data less well than their peaks-biased or C/O-biased counterparts. The slice plots of density-biased models (Figure 2) share the ‘bubbly’ appearance of the CfA2 slices, but the model voids are considerably larger than those in the CfA2 survey.

Most of the unbiased, peaks-biased, and C/O-biased models of Figure 9 match the VGH data fairly well. Unbiased models typically fit best at small \bar{d} , while peaks-biased or C/O-biased models

fit better at larger \bar{d} , with $b \approx 1.5 - 2$ models perhaps the most successful overall. Among unbiased and peaks-biased models, the data do not seem to strongly prefer any one of our three $(\Gamma, \Omega_0, \lambda_0) = (0.5, 1, 0), (0.25, 1, 0), (0.25, 0.3, 0.7)$ parameter combinations. The high- Γ models fit better at $\bar{d} = 5.6 h^{-1}\text{Mpc}$, but they underproduce large voids at $\bar{d} = 10.9 h^{-1}\text{Mpc}$, where the low- Γ models are more successful. All of our biased models overestimate the VPF at $\bar{d} = 5.6 h^{-1}\text{Mpc}$, while all of our unbiased models underestimate the VPF at $\bar{d} = 10.9 h^{-1}\text{Mpc}$, so no one model offers an ideal fit to the data. However, we have not yet considered the effects of finite volume errors, so we cannot draw quantitative conclusions.

3.5 Error Estimates for Specific Models

Although the CfA2 survey is one of the deepest and most ambitious redshift surveys to date, the total volume that it probes does not exceed the volume of the largest low density regions by an enormous factor. Estimates of the VPF are therefore subject to significant finite volume errors — a distant observer mapping a volume of the universe of the same size might find a different VPF because of statistical fluctuations in the local structure. These finite volume effects dominate over other sources of error (*e.g.*, magnitude and redshift errors) in the observed VPF. To decide whether a particular theoretical model is consistent with the VGH data, we must ask whether observers mapping equal volumes of the model universe could reproduce the observed VPF a reasonable fraction of the time.

The best way to carry out such a comparison between simulations and data is to draw from the numerical models simulated data sets with the same geometry and selection effects as the observational survey, then analyze the simulated and real data in an identical fashion. We do not know precisely what procedures VGH used for defining their samples and placing their test spheres, so here we adopt the simpler procedure of analyzing spherical samples with the same volumes as the VGH samples. This method should still yield reasonable estimates of the finite volume fluctuations for each sample. Within each of the two simulations of a given model, we place 50 ‘observers’ (*i.e.*, origins) at random positions. Around each observer in turn, we move the particles into redshift space and measure the VPF in eight spherical samples, with volumes chosen to match those of VGH’s eight volume-limited CfA2 samples. The radii R_{sample} of these spheres range from $22.9 h^{-1}\text{Mpc}$ (giving the volume of the $\bar{d} = 4.5 h^{-1}\text{Mpc}$, CfA2 North sample) to $54.7 h^{-1}\text{Mpc}$ (giving the volume of the $\bar{d} = 10.9 h^{-1}\text{Mpc}$, CfA2 South sample). In each sample sphere we randomly select a fraction $(4.5 h^{-1}\text{Mpc}/\bar{d}_s)^3$ of the particles, where \bar{d}_s is the characteristic separation of the associated CfA2 sample, so that on average the mean galaxy density in our samples matches that of observed galaxies at the associated absolute magnitude limit. We measure the redshift-space VPF by counting galaxies in spheres of radius $1, 2, \dots, R_{\text{max}} h^{-1}\text{Mpc}$, placed at 8000 random positions out to a distance $(R_{\text{samp}} - R_{\text{max}})$ from the observer. We adopt $R_{\text{max}} = 12, 14, 16,$ and $22 h^{-1}\text{Mpc}$ for the four successive values of \bar{d} . These values are large enough to go beyond the largest voids found by VGH at each \bar{d} . The larger R_{max} , the smaller the volume we have in which to place test spheres, so we always attempt to keep R_{max} significantly smaller than R_{sample} .

Our procedure produces 100 ($= 50$ observers per realization $\times 2$ realizations) measures of the VPF for each of the eight CfA2 sample volumes, and we sort these 100 measures from the lowest to the highest VPF at each radius R . The 5th, 25th, 75th, and 95th positions in this ranking represent our best estimates of the 5%, 25%, 75%, and 95% VPFs associated with a given model. At a given radius, one out of 20 observers measures a VPF value lower than the 5% VPF, and one out of 20 measures a VPF higher than the 95% VPF. Half of the observers measure a VPF between the 25% and 75% levels. If the observational data fall in this inter-quartile range, then the model

matches the data well. If the data fall in the 5%–95% range, then the model and data agree at the “ 2σ ” level. Successive points on the VPF are not independent, since a large void at one radius must contain voids at all smaller radii. VPFs at different \bar{d} are also not independent because a void that is empty at one \bar{d} must be empty at all larger \bar{d} . These interdependences make it difficult to combine multiple VPF measurements for multiple samples into overall model likelihoods. We will not attempt to solve this statistical problem in this paper; we leave the task of devising useful likelihood tests to a more detailed comparison study that applies matched procedures to simulations and observations.

We cannot attach “error bars” directly to the observational data in a model-independent way because we do not know the underlying statistical distribution from which the real data are drawn. The expected finite-volume errors are different for each theoretical model — models with larger voids also have larger sample-to-sample fluctuations in the VPF — so we must compare the data individually to each model in turn. Figures 10a, 10b, and 10c show such a comparison for three cases that span the range of our ‘ Γ ’ model VPFs: the unbiased, $(\Gamma, \Omega_0, \lambda_0) = (0.25, 0.3, 0.7)$ model, the $b = 1.5$, C/O-biased, $(\Gamma, \Omega_0, \lambda_0) = (0.5, 1, 0)$ model, and the $b = 3$, density-biased, $(\Gamma, \Omega_0, \lambda_0) = (0.25, 1, 0)$ model. The first of these is a representative unbiased model, the second is arguably the most physically motivated of our biased models, and the third creates the largest voids of all our ‘ Γ ’ models. Left and right hand columns of Figure 10 are associated with the sample volumes of ‘CfA2 North’ and ‘CfA2 South’, respectively, and the four rows correspond to $\bar{d} = 4.5, 5.6, 7.4,$ and $10.9 h^{-1}$ Mpc, from top to bottom. Circles (left hand columns) and asterisks (right hand columns) show the VGH data. The pair of solid lines in each panel shows the 5% and 95% VPFs of the corresponding model; the region between them can be regarded as a “ 2σ error corridor” for the model. The pair of dotted lines shows the 25% and 75% VPFs. Both pairs of lines diverge as P_0 descends because of the logarithmic scale on the P_0 -axis.

Beginning with Figure 10a, we see that the VGH data generally lie between the 75% and 95% VPFs of the unbiased, $(\Gamma, \Omega_0, \lambda_0) = (0.25, 0.3, 0.7)$ model. Although the model systematically underproduces large voids on average, it is consistent with the data at the 2σ level. The only exception is the large- R tail of the $\bar{d} = 4.5 h^{-1}$ Mpc, northern VPF, which lies slightly above the model’s 95% VPF. This tail is the one region of qualitative discrepancy between the VPFs of the CfA2 North sample and the corresponding VPFs of the other two VGH samples, so we are reluctant to place much weight on it. Putting it aside, we conclude that the VGH data are consistent with an unbiased Gaussian model, and that the voids in the CfA2 survey provide no convincing evidence for biased galaxy formation.

Figure 10b shows still better agreement between model and data. Most of the VGH results lie between the 25% and 75% VPFs of this $b = 1.5$, C/O-biased, standard CDM model. Again the tail of the $\bar{d} = 4.5 h^{-1}$ Mpc, northern VPF lies just above the model’s 95% VPF. Apart from this discrepancy, the VGH data agree well with this Gaussian model, which incorporates the sort of modest bias predicted by cosmological simulations with gas dynamics (CO; Katz *et al.* 1992). Similar results obtain for peaks-biased models.

Figure 10c shows results for our most severely biased ‘ Γ ’ model. For $\bar{d} \leq 7.4 h^{-1}$ Mpc, the VGH data lie mostly between the 5% and 25% VPFs, confirming the tendency of this model to overproduce large voids. However, even though the mean VPF predicted by this model is a poor match to the data (see Figure 9b), the model remains consistent with the current observations because it predicts large VPF variations in samples of this size. This is probably a specific example of a general problem: models with large voids also have large sample-to-sample fluctuations in the VPF, so larger data sets are needed to rule them out.

The overall message of this section may seem somewhat discouraging. The data do not convincingly exclude any of these three models, even though the models span a large range in predicted

Figure 10a

obtain by request (3 x 112 kb)

Figure 10 — Detailed comparison between three of our models and the VGH data, including the effects of finite volume fluctuations. Circles (left panels) and asterisks (right panels) show the VGH data from ‘CfA2 North’ and ‘CfA2 South,’ respectively, with $\bar{d} = 4.5, 5.6, 7.4,$ and $10.9 h^{-1}\text{Mpc}$ from top to bottom. For each of these eight samples, we measure the VPF from 100 simulated data sets drawn from the theoretical model, each with the same volume as the corresponding observational sample. Solid lines in each panel mark the 5th-lowest and 5th-highest VPFs of the 100 model data sets; the region between them can be regarded as a “ 2σ error corridor” for the model. Dotted lines mark the 25th-lowest and 25th-highest VPFs, and thus represent the model’s inter-quartile range. (a) The unbiased, $(\Gamma, \Omega_0, \lambda_0) = (0.25, 0.3, 0.7)$ model. The data are consistent with the model at the “ 2σ ” level, except for the large- R tail in the northern, $\bar{d} = 4.5 h^{-1}\text{Mpc}$ sample. (b) The $b = 1.5$, C/O-biased, $(\Gamma, \Omega_0, \lambda_0) = (0.5, 1, 0)$ model. This model provides an excellent fit to the data overall, though again there is a small area of discrepancy in the tail of the northern, $\bar{d} = 4.5 h^{-1}\text{Mpc}$ sample. (c) The $b = 3$, density-biased, $(\Gamma, \Omega_0, \lambda_0) = (0.25, 1, 0)$ model. Although the model tends to overproduce voids at the smaller values of \bar{d} , it predicts large sample-to-sample variations in the VPF (wide error corridors), so it cannot be ruled out by the current data.

Figure 10b

Figure 10 — *continued*

VPFs. However, the situation should improve in the near future, as the CfA extension has now been completed over a larger fraction of the sky. M. Vogeley (private communication) reports that VGH have now doubled the size of their observational sample, and that the VPF results for this larger sample are similar to those for the original data set. With the doubled sample, it may well be possible to rule out severely biased models, and perhaps even unbiased models. In the longer run, massive redshift surveys like the Sloan Digital Sky Survey (Gunn & Knapp 1993) will probe much greater volumes and yield highly accurate estimates of the VPF, placing correspondingly tight constraints on theories of biased galaxy formation.

Figure 10c

Figure 10 — *continued*

3.6 The Probability Function of Underdense Regions

Figure 11 illustrates the ‘underdense probability function’ $P_{80}(R)$ for a variety of our ‘ Γ ’ models. Its three rows display redshift-space UPFs for our $(\Gamma, \Omega_0, \lambda_0) = (0.5, 1, 0)$, $(0.25, 1, 0)$, and $(0.25, 0.3, 0.7)$ models, from top to bottom. The figure’s columns and line types have the same biasing associations as Figure 9’s (including the association of the dot-dashed line in the top right panel with $b = 1.5$, C/O biasing). Since it is always easier to find an 80% underdense region than a totally empty one, the UPFs have higher amplitudes at a given radius than their corresponding VPFs (cf. Figure 9). Also, these redshift-space UPFs – like redshift-space VPFs – are somewhat

Figure 11

obtain by request (120 kb)

Figure 11 — The underdense probability functions (UPFs) of our ‘ Γ ’ models. $P_{80}(R)$ is the probability that the average galaxy density within a randomly placed sphere of radius R (in h^{-1} Mpc) is more than 80% below the global mean density. Unlike the VPF, the UPF is independent of the space density of the tracer population, except for shot noise. In each panel, solid, dotted, short-dashed, and long-dashed lines represent UPFs for models with $b = 1, 1.5, 2,$ and $3,$ respectively. The $b \geq 1.5$ lines in the left and right columns are associated with peaks biasing and density biasing, respectively. The dot-dashed line in the upper right panel represents the $b = 1.5,$ C/O-biased model. The model parameters $\Gamma, \Omega_0,$ and λ_0 are listed in each panel.

larger than their real-space counterparts (cf. Figure 3).

Figure 11 confirms several of the \bar{d} -independent trends of Figure 9. For example: (i) density biasing produces significantly larger voids than peaks biasing; (ii) peaks biasing and C/O biasing produce statistically similar voids; (iii) among biased models, the sizes of voids generally increase as Γ is lowered; (iv) the differences in void structure between $b = 1$ and $b = 1.5$ models can be much larger than those among $b \geq 1.5$ models, and this effect is stronger among models with more large-scale power. The UPF of unbiased models increases with increasing large-scale power, *i.e.*, it is higher for lower Γ . WC found a similar result for power-law models. This trend is opposite to that of the unbiased VPF (again consistent with WC).

One advantage of the UPF over the VPF is its simplicity. It is independent of galaxy density, except for shot noise, which becomes progressively less important at larger radii. As a result, a single UPF can be measured directly from magnitude-limited data, without defining multiple volume-limited samples that have multiple values of \bar{d} . (However, additional complications enter if galaxy clustering depends systematically on luminosity.) Because the UPF falls more slowly with radius than the VPF, it can be measured out to larger scales in a given observational sample. We

do not know of any existing observational data on the UPF, so the curves in Figure 11 will have to stand as blind predictions. UPF results from the CfA2 survey should be available in the near future (M. Vogeley, private communication).

4. Conclusions

We have investigated the behaviour of the void probability function (VPF) in a wide range of initially Gaussian models for the origin of large-scale structure. We have focused on the sensitivity of the VPF to assumptions about biased galaxy formation. Our main conclusions about the dependence of the VPF on model parameters are as follows.

1. Peculiar velocity distortions have relatively little effect on the VPF, though VPFs measured in redshift space tend to be slightly higher than those measured in real space.
2. The real-space VPF is extremely insensitive to the cosmic density parameter Ω_0 and the cosmological constant λ_0 , provided that models with different values of these cosmological parameters have the same initial power spectrum and biasing prescription and are normalized to the same rms mass fluctuation at the present epoch.
3. In the absence of biasing, the VPF depends only weakly on the shape of the initial power spectrum, provided that models are normalized to $\sigma_{8,\text{mass}} \approx 1$ today. Unbiased models with more small-scale power have slightly higher VPFs.
4. The VPF is quite sensitive to the prescription adopted for biased galaxy formation. Density-biased models produce much larger voids than peaks-biased models, or models that incorporate CO's non-linear biasing prescription. Peaks-biased models have higher VPFs than unbiased models.
5. The VPF depends more strongly on the form of the biasing prescription (*e.g.*, density biasing versus peaks biasing) than on the bias factor b ; for a given biasing scheme, the VPF does not change much in the range $1.5 \leq b \leq 3$. Given the physical uncertainty in the appropriate choice of biasing scheme, the VPF is probably not a useful tool for determining b . However, the VPF can distinguish unbiased models from some biased models, and it can place useful constraints on the relation between galaxies and mass.
6. Conclusions 1 – 5 also apply to the underdense region probability function (UPF), except that the trend of the unbiased VPF with power spectrum (conclusion 3) is reversed for the UPF.

We have compared our model predictions to the data of VGH, who have measured VPFs of the original CfA survey and the completed regions of the CfA extension. Our main conclusions from comparison between models and the VGH data are as follows.

7. Unbiased Gaussian models reproduce the observed VPFs fairly well. The void probability data from the CfA survey do not provide compelling evidence for biased galaxy formation.
8. Models that incorporate moderate levels of biasing, similar to those predicted by cosmological simulations with gas dynamics, produce the best overall fit to the VGH data.
9. Density-biased models tend to overproduce large voids, at least on average.
10. Large finite volume fluctuations are expected in samples of the size analyzed by VGH, and models that predict the largest voids also predict the largest sample-to-sample variations in the VPF. As a result, the VGH data do not convincingly rule out any of our models.

The opening paragraph of this paper posed two broad questions. Can the gravitational growth of Gaussian primordial fluctuations account for the observed voids, or do initially Gaussian models

require that galaxy formation be suppressed in low density regions in order to produce voids as large and empty as observed? Do voids represent regions where there is no mass, or merely regions where there are no (bright) galaxies? Conclusion (10) tells us that we cannot offer convincing answers to these questions with the present observational data, at least not using the VPF as our primary tool. The VGH data are consistent with the hypothesis that voids in the CfA survey grew gravitationally from Gaussian primordial fluctuations, and that these voids are truly as underdense in mass as they are in galaxies. However, the data also permit a substantial bias between galaxies and mass, with the voids underdense, but not nearly so empty as they appear. Analysis of future redshift surveys will help to distinguish these possibilities.

Acknowledgments

We are grateful to Michael Vogeley for helpful discussions about the CfA results and for providing us with the VGH data in convenient form. We are also grateful to Changbom Park for allowing us to use his PM code, and to Renyue Cen for computing the parameters of equation (1) for our cubic cell filter. BL acknowledges the support of the Institute of Astronomy in Cambridge and a SERC postdoctoral fellowship. DHW is a W.M. Keck Foundation fellow at the Institute for Advanced Study. He acknowledges additional support from the Ambrose Monell Foundation and from the U.S. National Science Foundation in the form of grant PHY92-45317 and a NATO postdoctoral fellowship to Cambridge University, where this work began.

References

- Bardeen, J. M., Bond, J. R., Kaiser, N. & Szalay, A. S., 1986. *Astrophys. J.*, **304**, 15 (BBKS).
- Betancort-Rijo, J., 1990. *Mon. Not. R. astr. Soc.*, **246**, 608.
- Bhavsar, S. P., Gott, J. R. & Aarseth, S. J., 1981. *Astrophys. J.*, **246**, 656.
- Bond, J. R. & Efstathiou, G., 1991. *Phys. Lett. B*, **265**, 245.
- Bouchet, F., Strauss, M. A., Davis, M., Fisher, K. B., Yahil, A. & Huchra, J. P., 1993. submitted to *Astrophys. J.*
- Cen, R. & Ostriker, J. P., 1992. *Astrophys. J. Lett.*, **399**, L113.
- Cen, R. & Ostriker, J. P., 1993. Princeton Observatory Preprint POP-493, submitted to *Astrophys. J.* (CO).
- Cole, S. & Kaiser, N., 1989. *Mon. Not. R. astr. Soc.*, **237**, 1127.
- Davis, M., Efstathiou, G., Frenk, C. S. & White, S. D. M., 1985. *Astrophys. J.*, **292**, 371 (DEFW).
- Davis, M., Huchra, J., Latham, D. W. & Tonry, J., 1982. *Astrophys. J.*, **253**, 423.
- Davis, M. & Peebles, P. J. E., 1983. *Astrophys. J.*, **267**, 465.
- Davis, M., Summers, F. J. & Schlegel, D., 1992. *Nature*, **359**, 393.
- Davis, R.L., Hodges, H. M., Smoot, G. F., Steinhardt, P. J. & Turner, M. S., 1992. *Phys. Rev. Lett.*, **69**, 1856.
- Dekel, A. & Rees, M. J., 1987. *Nature*, **326**, 455.
- Dekel, A. & Silk, J., 1986. *Astrophys. J.*, **303**, 39.
- de Lapparent, V., Geller, M. J. & Huchra, J. P., 1986. *Astrophys. J. Lett.*, **302**, L1.
- de Lapparent, V., Geller, M. J. & Huchra, J. P., 1991. *Astrophys. J.*, **369**, 273.
- Doroshkevich, A. G., Kotok, E. V., Novikov, I. D., Polyudov, A. N., Shandarin, S. F., & Sigov, Yu. S., 1980. *Mon. Not. R. astr. Soc.*, **192**, 321.
- Dressler, A., 1980. *Astrophys. J.*, **236**, 351.
- Dubinski, J., da Costa, N., Goldwirth, D. S., Lecar, M. & Piran, T., 1993. *Astrophys. J.*, in press.
- Efstathiou, G., Bond, J. R. & White, S. D. M., 1992. *Mon. Not. R. astr. Soc.*, **258**, 1P (EBW).
- Efstathiou, G., Davis, M., Frenk, C. S. & White, S. D. M., 1985. *Astrophys. J. Supp.*, **57**, 241.
- Efstathiou, G., Kaiser, N., Saunders, W., Lawrence, A., Rowan-Robinson, M., Ellis, R. S. & Frenk, C. S., 1990. *Mon. Not. R. astr. Soc.*, **247**, 10P.
- Einasto, J., Einasto, M., Gramann, M. & Saar E., 1991. *Mon. Not. R. astr. Soc.*, **248**, 593 (EEGS).
- Evrard, A. E., Summers, F. J. & Davis, M., 1993. submitted to *Astrophys. J.*
- Fisher, K. B., Davis, M., Strauss, M. A., Yahil, A. & Huchra, J. P., 1993. *Astrophys. J.*, **402**, 42.
- Fry, J. N., 1986. *Astrophys. J.*, **306**, 358.
- Fry, J. N., Giovanelli, R., Haynes, M. P., Melott, A. L., & Scherrer, R. J., 1989. *Astrophys. J.*, **340**, 11.
- Gelb, J. M., 1992. *Ph.D. thesis*, MIT.
- Geller, M. J. & Huchra, J. P., 1989. *Science*, **246**, 897.

- Gott, J. R., Mao, S., Park, C., & Lahav, O., 1992. *Astrophys. J.*, **385**, 26.
- Gott, J. R., Melott, A. L. & Dickinson, M., 1986. *Astrophys. J.*, **306**, 341.
- Gott, J. R. *et al.*, 1989. *Astrophys. J.*, **340**, 625.
- Gott, J. R. & Rees, M. J., 1975. *Astr. Astrophys.*, **45**, 365.
- Gott, J. R. & Turner, E. L., 1977. *Astrophys. J.*, **216**, 357.
- Gregory, S. A. & Thompson, L. A., 1978. *Astrophys. J.*, **222**, 784.
- Gunn, J. E., 1982. In: *Astrophysical Cosmology*, p.233, eds Brück, H. A., Coyne, G. V. & Longair, M. S., Specola Vaticana, Rome.
- Gunn, J. E. & Knapp, G. R., 1993. In: *Astronomical Surveys*, ed Soifer, B. T., ASP conference proceedings, in press.
- Haynes, M. P. & Giovanelli, R., 1986. *Astrophys. J. Lett.*, **306**, L55.
- Haynes, M. P. & Giovanelli, R., 1988. In: *Large-Scale Motions in the Universe*, p. 31, eds Rubin, V. C. & Coyne, G. V., Princeton University Press, Princeton.
- Hernquist, L., Bouchet, F. R. & Suto, Y., 1991. *Astrophys. J. Supp.*, **75**, 231.
- Huchra, J. P., Davis, M., Latham, D. & Tonry, J., 1983. *Astrophys. J. Supp.*, **52**, 89.
- Joeveer, M. & Einasto, J., 1978. In: *The Large Scale Structure of the Universe, IAU Symposium 79*, p. 241, eds Longair, M. S. & Einasto, J., Reidel, Dordrecht.
- Kaiser, N., 1984. *Astrophys. J. Lett.*, **284**, L9.
- Kaiser, N., 1988. In: *Evolution of Large Scale Structures in the Universe, IAU Symposium 130*, p. 43, eds Audouze, J. & Szalay, A., Reidel, Dordrecht.
- Katz, N., Hernquist, L. & Weinberg, D. H., 1992. *Astrophys. J. Lett.*, **399**, L109.
- Katz, N., Quinn, T. & Gelb, J. M., 1993. submitted to *Mon. Not. R. astr. Soc.*.
- Kauffmann, G. & Melott, A. L., 1992. *Astrophys. J.*, **393**, 415.
- Kirshner, R. P., Oemler, A., Schechter, P. L. & Shectman, S. A., 1981. *Astrophys. J. Lett.*, **248**, L57.
- Kirshner, R. P., Oemler, A., Schechter, P. L. & Shectman, S. A., 1987. *Astrophys. J.*, **314**, 493.
- Klypin, A., Holtzman, J., Primack, J. & Regös, E., 1993. submitted to *Astrophys. J.*.
- Lachièze-Rey, M., da Costa, L. N. & Maurogordato, S., 1992. *Astrophys. J.*, **399**, 10.
- Liddle, A. R. & Lyth, D. H., 1992. *Phys. Lett. B*, **291**, 391.
- Lidsey, J. E. & Coles, P., 1992. *Mon. Not. R. astr. Soc.*, **258**, 57P.
- Lucchin, F., Mataresse, S. & Mollerach, S., 1992. *Astrophys. J. Lett.*, **401**, L49.
- Maddox, S. J., Efstathiou, G., Sutherland, W. J. & Loveday, J., 1990. *Mon. Not. R. astr. Soc.*, **242**, 43P.
- Maurogordato, S. & Lachièze-Rey, M., 1987. *Astrophys. J.*, **320**, 13.
- Melott, A. L., 1986. *Phys. Rev. Lett.*, **56**, 1992.
- Moore, B., Frenk, C. S., Weinberg, D. H., Saunders, W., Lawrence, A., Ellis, R. S., Kaiser, N., Efstathiou, G. & Rowan-Robinson, M., 1992. *Mon. Not. R. astr. Soc.*, **256**, 477.
- Narlikar, J. V. & Padmanabhan, T., 1991. *Annu. Rev. Astron. Astrophys.*, **29**, 325.
- Park, C., 1990. *Ph.D. thesis*, Princeton University.

- Park, C., 1991. *Mon. Not. R. astr. Soc.*, **251**, 167.
- Postman, M. & Geller, M.J., 1984. *Astrophys. J.*, **281**, 95.
- Rees, M. J., 1985. *Mon. Not. R. astr. Soc.*, **213**, 75P.
- Regös, E. & Geller, M. J., 1991. *Astrophys. J.*, **377**, 14.
- Rood, H. J., 1988. *Annu. Rev. Astron. Astrophys.*, **26**, 245.
- Salopek, D. S., 1992. *Phys. Rev. Lett.*, **69**, 3602.
- Saunders, W., Frenk, C., Rowan-Robinson, M., Efstathiou, G., Lawrence, A., Kaiser, N., Ellis, R., Crawford, J., Xia, X. Y. & Parry, I., 1991. *Nature*, **349**, 32.
- Silk, J., 1985. *Astrophys. J.*, **297**, 1.
- Smoot, G. F. *et al.*, 1992. *Astrophys. J. Lett.*, **396**, L1.
- Souradeep, T. & Sahni, V., 1992. *Mod. Phys. Lett. A*, **7**, 3541.
- Taylor, A. N. & Rowan-Robinson, M., 1992. *Nature*, **359**, 396.
- van de Weygaert, R. & van Kampen, E., 1993. *Astrophys. J.*, in press.
- Vogeley, M. S., Geller, M. J. & Huchra, J. P., 1991. *Astrophys. J.*, **382**, 44 (VGH).
- Vogeley, M. S., Park, C., Geller, M. J. & Huchra, J. P., 1992. *Astrophys. J. Lett.*, **391**, L5.
- Weinberg, D. H. & Cole, S., 1992. *Mon. Not. R. astr. Soc.*, **259**, 652 (WC).
- Weinberg, D. H. & Gunn, J. E., 1990. *Mon. Not. R. astr. Soc.*, **247**, 260.
- West, M. J., Weinberg, D. H. & Dekel, A., 1990. *Astrophys. J.*, **353**, 329.
- White, S. D. M., 1979. *Mon. Not. R. astr. Soc.*, **186**, 145.
- White, S. D. M., Davis, M., Efstathiou, G. & Frenk, C. S., 1987. *Nature*, **330**, 451.